Direct Measurement of Depletion Force between Two Surfaces with Total Internal Reflection Microscopy

XING, Xiaochen

A Thesis Submitted in Partial Fulfillment
of the Requirements for the Degree of
Master of Philosophy
in
Chemistry

The Chinese University of Hong Kong
July 2009

Thesis / Assessment Committee

Professor NGAI, To (Supervisor)

Professor CHAN, Man Chor (Chairman)

Professor ZHENG, Bo (Committee Member)

Professor ZHANG, Guangzhao (External Examiner)

摘要

摘要

在膠體粒子和長鏈高分子的混閤體繫中，如果高分子的呎吋超過膠體粒子與粒子間的空間呎吋，那么膠體粒子可以引導一种吸引力---“排空力”。這是熵驅動過程。當高分子鏈避開膠體粒子間的空間時可以對應著更少的搆象熵，那么粒子間的縫隙內外將會齣現滲透壓的不平衡從而導緻膠體粒子間的吸引作用。關於排空力的課題自從 1980 年開始被科學界關注后逐漸發展到在多種不同體系內對其進行研究，其中包括：非吸附的納米粒子體系，表面活性劑的膠束溶液，高分子溶液以及電解質溶液。但是，至今為止對排空力進行直接的測量在實驗上仍然是個挑戰，其主要原因在于排空力的大小範圍基本在 10 至 100 非牛之間，即測量的能量波動精度必須保持在幾個 k_BT 內。

本文主要講述利用我們新搭建的全內反射顯微鏡來直接測量一個自由運動的聚苯乙烯粒子（半徑大約 3.2 微米）和一個平面間的相互作用。我們分別在兩種不同的體繫中研究它們之間的相互作用，一是水溶性的 PEO-PPO-PEO 三嵌段共聚物溶液，另一個是含有 PNIPAM 微凝膠粒子的分散溶液。我們的結果顯示當溶液離子濃度比較低的時候，PEO-PPO-PEO 溶液中可以形成納米氣泡，推測其穩定形成的原因是兩親性的 PEO-PPO-PEO 在氣/液介面進行了選擇性吸附。更重要的是，納米氣泡的存在引導了一個很有意義的排空力從而把PS粒子推向更靠近平面的位置。我們認為這個排空力來自于納米氣泡逃逸 PS 粒子與平面的縫隙時產生的不平衡的滲透壓，并最終導致了凈吸引的作用。

另外，我們合成了一種帶有 pH 值響應性的 PNIPAM 微凝膠粒子并研究了微凝膠粒子引導的粒子與平面的相互作用。應用 PNIPAM 微凝膠粒子的優點是可以通過改變改变 pH 值的大小而改變它的尺寸大小，從而方便我們直接測量由 pH 值變化而觸發的排空作用。實驗結果顯示在 PNIPAM 微凝膠粒子處於膨脹狀態時會在 PS 粒子與平面間引導一個吸引作用，而當 PNIPAM 微凝膠粒子處於塌縮狀態時這個吸引力則會消失。目前的研究證明了定量測量排空作用以及通過溶液 pH 值來控制排空力存在與消失的可行性，同時也為我們提供了一個利用可調的排空作用來引導膠體組裝的方法和途徑。

Abstract

Abstract

In a mixture of colloidal particles and long-chain polymers, particles may experience an attractive "depletion force" if the size of the polymers is larger than the inter-particle separation. This is an entropy-driven process. Individual polymers experience less conformational entropy if they stay between the particles so that they escape the inter-particle space, which results in an osmotic pressure imbalance inside and outside the gap and leads to inter-particle attraction. This depletion force has been the subject of several studies since the 1980s, and it has been investigated in the presence of nonadsorbing nanoparticle suspensions, surfactant micellar solutions, polymer solutions and in charged polyelectrolytes. The direct measurement of this force, however, is still experimentally challenging as it is normally in the range 10-100 fN, requiring the detection of energy variations of the order of k_BT and beyond.

In this thesis, we present our results for applying our newly established microscope, the Total Internal Reflection Microscopy (TIRM), to directly measure the interaction between a free-moving polystyrene (PS) sphere (radius ~3.2 μm) and a flat surface in an aqueous solution consisting of poly(ethylene oxide-*block*-propylene oxide-*block*-ethylene oxide) (PEO-PPO-PEO) triblock copolymer or poly(N-isopropylacrylamide) (PNIPAM) microgel particles. Our results reveal that when the solution ionic strength is low, nanobubbles can be spontaneously formed in the

PEO-PPO-PEO solution, presumably due to a preferential adsorption of amphiphilic PEO-PPO-PEO copolymer at the gas/water interface to stabilize the nanobubbles. Importantly, existence of these nanobubles creats a significant depletion force, pushing the PS sphere close to the flat surface. We suggest that the origin of such depletion attractive force comes from the exclusion or depletion of nanobubbles from the particle and flat surface gap, which leads to an osmotic pressure imbalance inside and outside the gap and results in the net attraction.

In addition, we have synthesized pH-responsive poly(N-isopropylacrylamide) (PNIPAM) microgel particles and investigated the microgel-induced interactions between a particle and a flat surface. One advantage of using these PNIPAM microgels as depletant is that the size of microgel particles can be reversibly tuned by lowering or raising the solution pH, which enables us to directly measure the depletion interaction triggered by a simple pH variation. We show that such pH-responsive microgel particles induce an attraction between the PS sphere and the flat surface at its swollen state. This attractive force, however, disappears as soon as the microgels are collapsed. The present study demonstrates the ability to quantitatively measure and reversibly control k_BT-scale depletion attraction as function of solution pH. Therefore, it offers a promising route to use such tunable depletion interactions in creating complex colloidal assemblies.

Content

Table of contents

Chapter 1

Introduction and background

Chapter 2

Principle of Total Internal Reflection Microscopy (TIRM) and Instrumentation

Chapter 3

Depletion Attraction between a Polystyrene Sphere and a Hydrophilic Surface in a Pluronic Aqueous Solution

Chapter 4

pH-Controllable Depletion Attraction Induced by Microgel Particles

Acknowledgment

Acknowledgement

At the beginning, I would like to express my sincere thanks to my supervisor, Prof. To Ngai, for his helpful guidance and encouragement during the entire period of my study. I entered his group as a postgraduate student in year 2007 and during the last two years, I felt grateful and appreciated for his excellent guidance, and meanwhile deeply inspired by his dedicatory attitude to the research and life. The precious experiences I gained from him would be a great fortune in my life.

Also, I would like to thank Prof. Chi Wu and Prof. Bo Zheng for the springing up many illuminating discussions.

My sincere thanks are also given to my dear group members, for their friendship and assistance has left me many unforgettable memories. They are Ms. Xiangjun Gong, Mr. Xiaoling Wei, Mr. Zifu Li, Mr. Zhuo Ao, Mr. Zhongmin Shen, Ms. Jingyi Li. Also, I would like give my thanks to the group members from other two research groups for their kindly discussion and friendly help during my research. They are Dr. Fan Jin, Dr. Liangzhi Hong, Ms. Jing Ye, Ms. Hui Ge, Mr. Rui Deng, Ms. Yanan Yue, Ms. Shu Diao, Mr. Hong Zhao, Mr. Qianjin Chen, Mr. Xuechang Zhou, Ms. Xiaoju Tang, Mr.Zuoyan Han, Mr. Xiaohu Zhou and Ms. Yuefang Li.

My sincere thanks are also extended to all the staff members in the Department of

Physics and Chemistry, also the Chinese University of Hong Kong for the academic atmosphere and the service they offered.

Finally, I would like to give my best thanks to my parents for their endless love and strong moral support to me all the time.

Xiaochen Xing

Hong Kong, June, 2009

Chapter 1

Introduction and Background

1.1 Overview of Studies in Colloid-Polymer Mixture

The applications of colloidal particles in many industries often involve the use of polymers. Polymers may be adsorbed to the particles, chemically attached to their surfaces or be free in solution. Whatever form polymers take, their presence has a major effect on the stability of colloidal dispersions. As a result, the study of colloid-polymer mixture is an area of active research directly of interest to many industries.

To understand the effect of an additional polymer on colloidal interaction, the fundamental question is whether the polymer adsorbs at the particle surface or not. To act as stabilizers, polymers must adsorb or graft onto the surface of the particle which can lead to a steric or electrosteric repulsion. If the polymer chains do not adsorb onto the surfaces, an attractive "depletion force" between the dispersed particles might occur at low polymer concentrations.

1.2 Depletion Force in Colloid-Polymer mixture

Depletion interaction between colloidal spherical particles due to non-adsorbing

polymers is a subject that has gained an increasing attention since 1980s. Understanding depletion phenomena is relevant in many ways. Firstly, it helps to understand when and why phase separation occurs in mixtures of polymers and colloids, which are often jointly present in industrial applications. Besides these practical reasons, depletion studies provide an accessible way of changing the range of the interaction potential between the colloidal particles by varying the size. This is helpful for studying the properties of liquids, crystallization as well as gelation phenomena, using colloid system instead of low-molar-mass substances.

The mechanism that is responsible for depletion interaction can be explained on the level of a pair of spherical colloids immersed in a solution of non-adsorbing polymers as shown in Fig.1-1. When the surface of two large particles happen to approach within the diameter d of the polymer chains, the polymer can be excluded or depleted from the region between the two larger particles. In this way, this depletion results in an osmotic pressure gradient, which goes from a maximum polymer-segment concentration at the bulk to zero at the particle surface, i.e., the depletion region. For a single particle, the osmotic pressure is isotropic (Fig.1-1a). However, if the depletion layers overlap, the osmotic pressure becomes anisotropic and there is a net attractive force, as indicated by the arrows (Fig.1-1b). For ideal (the polymer segments do not 'feel' other segments) polymers, the effective free energy of interaction equals the overlap volume (indicated by the hatched region) multiplied by the osmotic pressure.

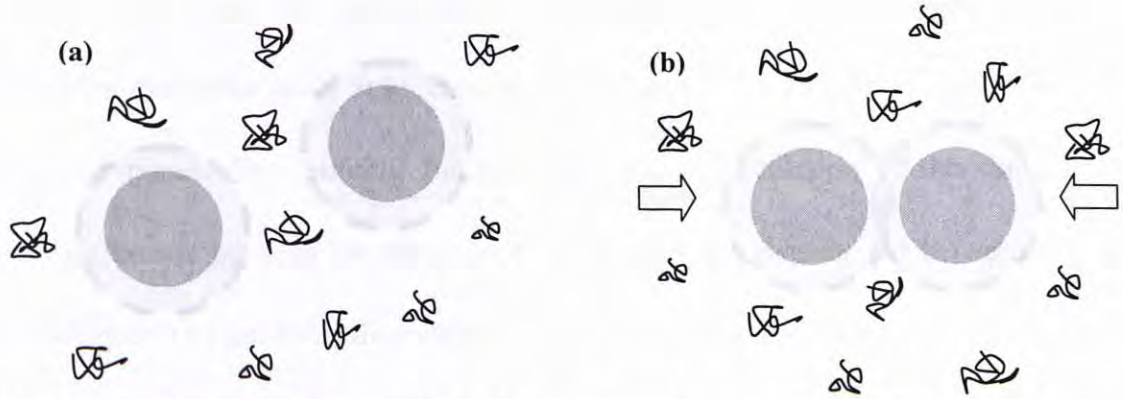

Fig.1-1 Schematic picture of two colloidal spheres in a polymer solution with non-adsorbing polymers. The depletion layers are indicated by short dashed. When there is no overlap (a) the osmotic pressure on the spheres due to the polymer solution is isotropic. For overlapping depletion layers (b) the osmotic pressure on the spheres is unbalanced; the excess pressure is indicated by the arrows.

1.2.1. Depletion Interaction in Monodisperse and Neutral Polymer–Colloid Mixtures: Theory

1.2.1.1. An Exact Result: the Interaction between Parallel Plates due to Ideal Polymer Chains

Theoretical progress on the depletion problem began in the late 1950s. In 1954, Asakura and Oosawa firstly indicated that two plates immersed in a solution of ideal non-adsorbing polymers attract one another [1]. Using statistical mechanics they derived an expression for the partition coefficient: namely, the polymer concentration between the plates divided by the concentration outside the plates, by solving the Edwards diffusion equation for polymers. It is worth to note that the term diffusion is used, as there is an analogy with a diffusion process. The random walk conformation of

a polymer chain can be described as a diffusion process. Consequently, the concentration difference leads to an expression for the pressure difference outside and between the plates. The partition function thus allows calculation of the osmotic pressure difference between the plates as a function of the distance (h) between the plates. Integration of this force then yields the interaction potential W(h).

1.2.1.2. Penetrable hard sphere (*PHS*) Approach

In order to extend the theory, Asakura and Oosawa [2] later on proposed to simplify of an ideal non-adsorbing polymer chain by replacing it with a penetrable hard sphere (PHS), also denoted as a non-additive hard sphere. A *PHS* is a sphere that is hard for a colloidal particle, but which can freely permeate through another PHS. This leads to a simple depletion potential between two spheres:

$$\frac{W(h)}{kT} = -\frac{2}{3}\pi n_p a_{PHS}^3 (1-\frac{h}{2a_{PHS}})^2 (2+\frac{3R}{a_{PHS}}+\frac{h}{2a_{PHS}}) \qquad (1.1)$$

where n_p is the bulk concentration of polymers, a_{PHS} is the radius of a PHS, and R is the radius of the colloidal particle. Note that the radius of a PHS (a_{PHS}) that enables the minimum of the PHS-induced interaction potential is of the order of magnitude of the radius of gyration (R_g) of the polymer. The PHS concept was also independently developed and extended by Vrij [3]. They showed that the interaction potential between two spheres mixing with ideal non-adsorbing polymer chains could be described using

the second osmotic virial coefficient B_2, which was related to the interaction potential via:

$$B_2 = 2\pi \int_0^\infty dr(1-\exp(-\frac{W(r)}{kT})) \tag{1.2}$$

where r is the center-to-center distance between the spheres.

In the early 1980s, Gast et al. [4] proposed a pair-wise perturbation theory of a mixture of colloids and PHSs by considering free engergy. This extension of the PHS theory made it possible to assign the nature (i.e. colloidal gaseous, liquid or solid state) of the coexisting phases. A semi-grand canonical treatment was proposed by Lekkerkerker [5], who took the polymer partitioning between the phases into account.

Meijer and Fenkel [6] used computer simulations to test on a dispersion of spheres immersed in a solution of ideal lattice polymer chains. Their results showed that for small values of a_{PHS}/R the agreement with the free volume PHS theory of Lekkerkerker et al. [8] is very good. Deviations, however, appear for larger values of a_{PHS}/R. It is clear that the properties of polymers are oversimplified when they are regarded as PHSs. Besides that, in the PHS model it is often to take the effective excluded volume of a polymer near a plate. Thus, for a_{PHS} a value of $2R_g/\sqrt{\pi}$ (or, as is often found in the literature, R_g) is usually taken, in agreement with the theory of Asakura and Oosawa [1]. Thermodynamically, the proper choice for a_{PHS} is the depletion layer thickness Δ. The depletion layer thickness is defined such that the negative adsorption around a sphere immersed in a polymer solution is identical to that

of a sphere in a dispersion with PHSs [7]. The quantity Δ can thus be calculated from the negative adsorption of polymer segments around the colloidal particle or from the free energy of immersion of a colloidal particle in a polymer solution [8]. In order to do so, the polymer density profile is required. The polymer density of ideal polymer segments near a single plate was calculated by Eisenriegler [9] and yielded $\Delta = 2R_g / \sqrt{\pi}$. Taniguchi et al. [10] and Eisenriegler et al. [11] calculated the ideal polymer concentration profile around a single sphere, leading to the following expression for the depletion layer thickness Δ as a function of

$q = R_g / R$:

$$\frac{\Delta}{R_g} = \frac{1}{q}[(1 + \frac{6q}{\sqrt{\pi}} + 3q^2)^{1/3} - 1] \tag{1.3}$$

Eq. (1.3) was recently derived by Louis et al. [8] from the free energy of immersing a sphere into an ideal polymer solution. For $R_g / R < 0.3$, Δ still is of the order of R_g, while it strongly decreases for $R_g / R > 0.3$. This clearly illustrates the limitations of the 'classical' PHS approach. It may thus be concluded that replacing the ideal polymers by PHSs with a radius of the order of R_g is only valid in the so-called 'colloid limit', where $R_g << R$.

1.2.2. Early Experimental Findings of Depletion Interaction

Experimental work dealing with depletion interaction was reported a long time

before Asakura and Oosawa [1] first gave a theoretical background for this phenomenon. It has been known for a long time that red blood cells tend to cluster at high concentrations of the blood serum proteins. By now it is well recognized that depletion can be used to explain erythrocyte aggregation and precipitation [12]. The microbiologist Beijerinck [13] tried to mix gelatin and starch and reported that these biopolymers could not be mixed. The phenomenon can now be regarded as very early detection of depletion induced demixing. In the beginning of the last century, Traube [14] showed that adding certain polysaccharides derived to aqueous latex dispersions led to a concentration of latex. Vester [15] published a review on ways to optimize the creaming speed of lattices. Cockbain [16] reported the enhanced creaming of oil droplets in a stabilized oilin-water emulsion when the surfactant concentration exceeded the critical micelle concentration. This phenomenon was left unexplained at the time, until Fairhurst et al. [17] made a connection with depletion interaction theories and suggested that the micelles play an identical role to non-adsorbing polymers. Recently, depletion forces have been investigated in the presence of nonadsorbing nanoparticle suspensions [18], surfactant micellar solutions [19,20], polymer solutions [21,22] and in charged polyelectrolytes [23,24]. These studies have confirmed the main features of the expected depletion interaction.

1.3 References and Notes

1. Asakura, S.; Oosawa, F. *J. Chem. Phys.* **1954**, *22*, 1255.
2. Asakura, S.; Oosawa, F. *J. Polym. Sci.* **1958**, 33, 183.
3. Vrij, A. *Pure Appl. Chem.* **1976**, 48, 471.
4. Gast, A.P.; Hall, C.K.; Russel, W.B., *J. Colloid Interface Sci.* **1983**, 96, 251.
5. Lekkerkerker, H.N.W., Colloids Surf. **1990**, 51, 419.
6. Meijer, E.J.; Frenkel, D., *J. Chem. Phys.* **1994**, 100, 6873.
7. Tuinier, R.; Lekkerkerker, H.N.W.; Aarts, D.G.A.L., *Phys. Rev. E.* **2002**, 65, 060801(R).
8. Louis, A.A.; Bolhuis, P.G.; Meijer, E.J.; Hansen, J.P., *J. Chem. Phys.* **2002**, 116, 10547.
9. Eisenriegler, E., *J. Chem. Phys.* **1983**, 79, 1052.
10. Taniguchi, T.; Kawakatsu, T.; Kawasaki, K., in: Kawasaki, K.; Kawakatsu, K.; Tokuyama, M., (Eds.), Slow Dynamics in Condensed Matter, AIP Conference Proceedings, vol. 256, New York, **1992**, p. 503.
11. Eisenriegler, E.; Hanke, A.; Dietrich, S, *Phys. Rev. E.* **1996**, 54, 1134
12. Bedell, S.E.; Booker, B.T., *Am. J. Med.* **1985**, 78, 1001.
13. Beijerinck, M.W., Zentr. Bakteriol. Parasitenkd. Infektionskr. **1896**, 2 (2), 697.
14. Traube, J., Gummi Zeitung **1925**, 39, 434.
15. Vester, C.F., Kolloid Z. **1938**, 84, 63.

16. Cockbain, E.G., Trans. *Faraday Soc.* **1952**, 48, 185.

17. Fairhurst, D.; Aronson, M.P.; Gum, M.L.; Goddard, E.D., *Colloids Surf.* **1983**, 7, 153.

18. Sharma, A.; Walz, J. Y. *J. Chem. Soc. Faraday Trans.* **1996**, 92, 4997.

19. Richetti, P.; Kekicheff, P.; *Phys. Rev. Lett.* **1992**, 68, 1951.

20. Sober, D. L.; Walz, J. Y. *Langmuir* **1995**, 11, 2352.

21. Milling, A. J; Kendall, K. *Langmuir* **2000**, 16, 5106.

22. Piech, M.; Walz, J. Y. *J. Phys. Chem. B* **2004**, 108, 9177.

23. Biggs, S.; Dagastine, R. R.; Prieve, D. C. *J. Phys. Chem. B* **2002**, 106, 11557.

24. Biggs, S.; Prieve, D. C.; Dagastine, R. R. *Langmuir*, **2005**, 21, 5421.

Chapter 2

Principle of Total Internal Reflection Microscopy (TIRM) and Instrumentation

2.1 Introduction of Total Internal Reflection Microscopy (TIRM)

The first Total Internal Reflection Microscope (TIRM) was established by D.C.Prieve etc.al in 1987 [1]. It is a new experimental technique for measuring weak colloidal interactions between a single microscopic particle and a flat plate in an aqueous or organic environment. One of the advantages of TIRM is that it is capable to measure the weak forces without touching the particle, and while the particle remains free to undergo Brownian motion during the measurement. In this sense, it is more characteristic to real situation systems. More generally, TIRM is a technique for directly monitoring the instantaneous separation distance between the sphere and the flat surface. It was invented initially for exactly precise determination of the distance from a particle to a near interface. From the equilibrium distribution of separations sampled by Brownian motion, the potential energy profiles can be obtained. Following the first demonstration of the applicability of TIRM to determination the colloidal interactions, various studies have been reported, including the direct measurements of the depletion forces induced by rigid particle [2-5], polyelectrolyte [6-7], and nanobubbles [8]; as

well as the steric repulsion induced by Pluronic (PEO-PPO-PEO triblock) [9-10], PEO brushes [11] and Van Der Waals interaction [12].

2.2 The Principle of TIRM Technique

2.2.1 Total Internal Reflection

Internal reflection occurs when light is incident from an optically dense medium at a plane interface (z = 0), into an optically less dense medium ($n_2<n_1$). Based on Snell's law, the refracted ray (θ_t) is bent away from the normal and moved toward the interface as the angle of incidence is increased. A critical angle of incidence, θ_c, arises at which the refracted ray is parallel to the interface,

$$\sin\theta_c = n_2 / n_1 = n_{21} \tag{2.1}$$

If the angle of incidence θ_i is further increased, i.e., $\theta_i > \theta_c$, Snell's law gives a complex angle of refraction

$$\begin{aligned} \sin\theta_t &= (n_1 / n_2)\sin\theta_i > 1 \\ \cos\theta_t &= (1-\sin^2\theta_t)^{1/2} = iu \end{aligned} \tag{2.2}$$

where u is real and positive. The solution of the wave equation satisfying the appropriate boundary conditions still has the general form of a linear polarized plane wave (LPPW)

$$E = E_{0t} e^{-i\omega t} \exp(i[(K_t \sin\theta_t)x + (K_t \cos\theta_t)z]) \tag{2.3}$$

where E_{ot} is the magnitude of the transmitted electric field at the interface and K_t is the magnitude of the transmitted wave vector K_t. Combined Eq.2.2 and 2.3, the electric field can be written as

$$E = E_{0t}e^{-i\omega t}\exp[(iK_t \sin\theta_t)x]\exp(-K_t uz) \tag{2.4}$$

Instead of the sinusoidal dependence on z, it is characteristic of a propagating wave. The electric field now decays exponentially with z. For this reason, this solution of the wave equation is called an evanescent wave. The intensity of the evanescent wave I_{ev} is equal to the time average of the magnitude of the Poynting vector Π

$$\begin{aligned} \prod &= E \times H = (1/\omega\mu)E^2 K \\ I_{ev} &= \langle | \Pi | \rangle \end{aligned} \tag{2.5}$$

Here for an evanescent wave in medium 2, K=K_t, and the components of the Eq.2.5 become

$$\begin{aligned} \Pi_x &= (1/\omega\mu)K_t(E)^2(1+u^2)^{1/2} \\ \Pi_z &= (1/\omega\mu)K_t(E)^2(iu) \end{aligned} \tag{2.6}$$

The above equations show that a real flow of energy occurs only parallel to the surface. The evanescent wave transports no energy normal to the interface. By a combination, the following dependence on distance from the interface is obtained:

$$\begin{aligned} I_{ev}(h) &= I_{ev}(0)\exp(-\beta h) \\ \beta &= (2K_t u) = \frac{4\pi}{\lambda_0}[(n_1 \sin\theta_1)^2 - n_2^2]^{1/2} \end{aligned} \tag{2.7}$$

where h is equal to the parameter z. β^{-1} is the penetration depth of the evanescent wave

intensity. β^{-1} is approximately 110nm in our TIRM setup because we set the angle of incidence at $\theta_1 \sim 70^\circ$.

Because of the exponential behavior, a small change in z axis produces a measurable change in the evanescent intensity. As the resolution of the detector, for example photomultiplier tube (PMT), is constant, we could find that the height resolution of the detected signal is higher as the distance become closer to the interface. We can demonstrate the sensitivity as follows: if the PMT we used to quantify the light intensity can realistically detect a 1% change in intensity, then according to the value β^{-1} = 110 nm, a 1% change in I corresponds to a ~1 nm change in h. In other words, we can detect changes in h of the order of 1nm. However, as the particle moves further from the interface, the comparable evanescent intensity change corresponding to the same 1 nm position change will be too small to be detected.

2.2.2 Details on Scattering of the Evanescent Wave

In the real TIRM measurement, we probe the intensity change due to the Brownian motion of the particle. Typically, we collect the elastic scattered intensity by the particle of the evanescent wave at around 90° spatial angle, which is not limited to a specific angle but a range due to different objective numerical aperture (or so-called N.A = $n \times \sin\mu$). In this way, the signal we collected is a integral from intensity at a certain degree from $(90-\mu)^\circ$ to $(90+\mu)^\circ$. The objective used has N.A = 0.50, corresponding to μ

~ 20°. The particle appears in the microscope as a bright spot on a dark field (see Fig.

(a)) with the intensity continually flickering brighter or dimmer depending on whether the particle moves closer or far away from the surface. We can understand this process by dividing into two steps: an evanescent wave is firstly generated as an incident light source under the total internal reflection at the interface, the produced evanescent wave is then scattered by a particle moving within the wave existing area. The detector, PMT, detects the elastic-scattered intensity of z axis around 90° from the evanescent wave in the n_2 medium. Thus the obtained signal is actually coupled with the height information and the dynamic position-correction information for a selected micron particle. In principle, from the TIRM experiments, we only get the particle height (distance) information. However, by sampling the photon number from PMT detector for a certain period of time, we finally get a serious of averaged photon numbers which are proportional to the intensity at a fixed-angle range during the sampling time.

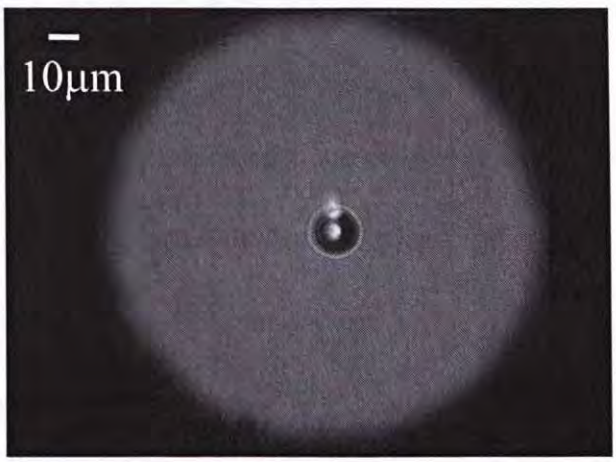

Fig.2-1(a) 10μm diameter PS sphere captured by CCD where it is illuminated by normal and evanescent light in our TIRM.

Elastic scattering without multiple reflections ($h \rightarrow \infty$)

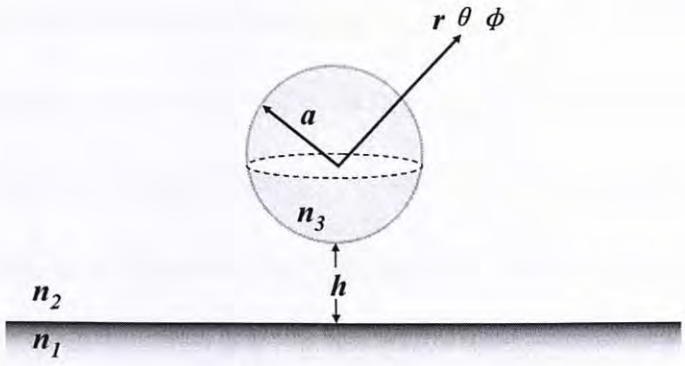

Fig.2-1(b) Sphereical particle acting as a scatterer of the evanescent wave produce at the plane. The scattered light is observed in the far-field limit at distance *r*.

Regarding to the scattering properties of an evanescent wave (see Fig.2-1(b)), Chew et al 13] have shown that for a non-adsorbing spherical particle located far enough from the surface and without multiple reflections of the evanescent wave, the scattered electric field has the far-field form (as $r \rightarrow \infty$) described as:

$$E_{sc}(r,\theta,\phi) = \exp(-\beta h/2)\frac{\exp(iK_1 r)}{K_1 r}\sum_{l,m} B_{l,m}(\theta,\phi) \tag{2.8}$$

where r, θ, φ are spherical coordinates at the origin of the sphere center and h is the separation distance between the sphere and the plate. The $B_{l,m}$ contains vector spherical harmonics, depending on the size of the sphere, the incident evanescent wave, and the refractive indices but is independent of h. The intensity of the scattered wave, which is proportional to E_{sc}^2, is given by

$$I_{sc}(h) = I_0 \exp(-\beta h) \tag{2.9}$$

where I_0 is a constant. It should be noted that Eq.2.9 is different with Eq.2.7, where the former is the scattered part of the followed one. Eq.2.9 can be used to interpret the signal from the PMT by assuming that the particle located far enough from the surface and without the multiple reflections. It should be noted that I_0 is not absolutely equal to $I_{sc}(h = 0)$. Some studies [14] showed the functional dependence of h failed when $\beta h <$ 1.5 due to the multiple reflections. Consequently, although $I_{sc}(0)$ could be directly measured by salting out the sphere, I_0 in Eq.2.9 cannot be deduced. The reason is that Eq.2.9 cannot be expected to hold for $\beta h << 1$.

2.2.3 Data Analysis

TIRM monitors the instantaneous separation distance, h, between the particle and the flat surface. After taking one measurement, we wait for the distance to change and take another measurement. By repeating this process at short interval (Δt = 1ms) for a certain time (15 mins), a statistically large number of times N ~ 900,000 was measured (Fig.2-2). Then, an intensity histogram can be obtained, which converges for infinite N to the probability density function, $p(h)$. In other words, $n(h)$ is directly proportional to $p(h)$ and the ratio of probabilities can be replaced by the ratio of the number of observations in the corresponding bins of the histogram. Consequently, the potential energy profile ($p(h)$) perpendicular to the interface can be deduced by evaluating the

Boltzmann's equation:

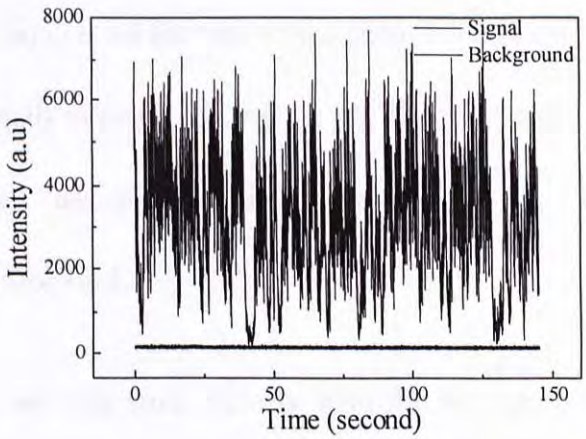

Fig.2-2 Fluctuations of signal and background in evanescent wave scattering observed for a 6-μm diatmer PS latex sphere in 0.1mM NaCl solution collected by our TIRM instrument.

$$p(h) = A\exp[-\frac{\Phi(h)}{kT}] \tag{2.10}$$

where A is the normalized constant. With $p(h)$ from the TIRM histogram, we can turn Eq.2.10 'inside-out' to deduce the potential energy profile $\Phi(h)$. Besides, in order to eliminate A, we divide p(h) by p(h_m) evaluated at a reference position denoted as h_m. According to Eq.2.10, this results in

$$\frac{\Phi(h)-\Phi(h_m)}{kT} = \ln\frac{p(h_m)}{p(h)} \tag{2.11}$$

where h_m is an arbitrary reference height, usually taken as the elevation corresponding to the minimum of $\Phi(h)$. So the potential profile can finally be deduced from the histogram using

$$\frac{\Phi(h)-\Phi(h_m)}{kT}=\ln\frac{n(h_m)}{n(h)} \tag{2.12}$$

Note that Eq 2.12 requires all the bins of the histogram $n(h)$ must have equal width Δh and Δh must be small enough, i.e., $\Delta h \rightarrow dh$. If each measurement of intensity I is separately converted into a corresponding elevation h, then construction of such a histogram is straightforward.

Alternatively, we can work directly with the histogram of the intensities $N(I)$, where $N(I)$ is the number of observations of intensity in the range from I to $I + \Delta I$. The probability density of intensity $P(I)$ can be related to the probability density of elevation $p(h)$ by considering that the number of observations of intensity in the range from I to $I + \mathrm{d}I$ is equal to the number of observations of elevation in the corresponding range from h to $h + dh$:

$$P(I)dI = p(h)dh \tag{2.13}$$

or further represented as

$$p(h) = P(I)\frac{dI}{dh} = -\beta P(I)I(h) \tag{2.14}$$

where the second equality is obtained with the help of Eq.2.10. One consequence of Eq.2.14 is that the most probable elevation is not equal to the elevation corresponding to the most probable intensity, although the two elevations typically differ by only a few nanometers. After substituting eq(1.14), Eq.2.11 becomes

$$\frac{\Phi(h)-\Phi(h_m)}{kT}=\ln\frac{N(I_m)I_m}{N(I)I} \tag{2.15}$$

where $I_m = I(h_m)$. If the histogram of intensities has bins of equal width ΔI, and if ΔI is small, then $P(I)$ and $P(I_m)$ can be replaced by $N(I)$ and $N(I_m)$, which has already been assumed in Eq.2.15. The extra factor I_m / I of the logarithm essentially accounts for having equal bin widths in intensity I, instead of equal bin widths in h. Besides having the intensity histogram and the potential energy profile, our standard data analysis procedure also includes the power spectral density (PSD) of both the signal and background after noise is removed, as well as the calculated time auto-correction curve of the scattering evanescent intensity (Fig.2-3).

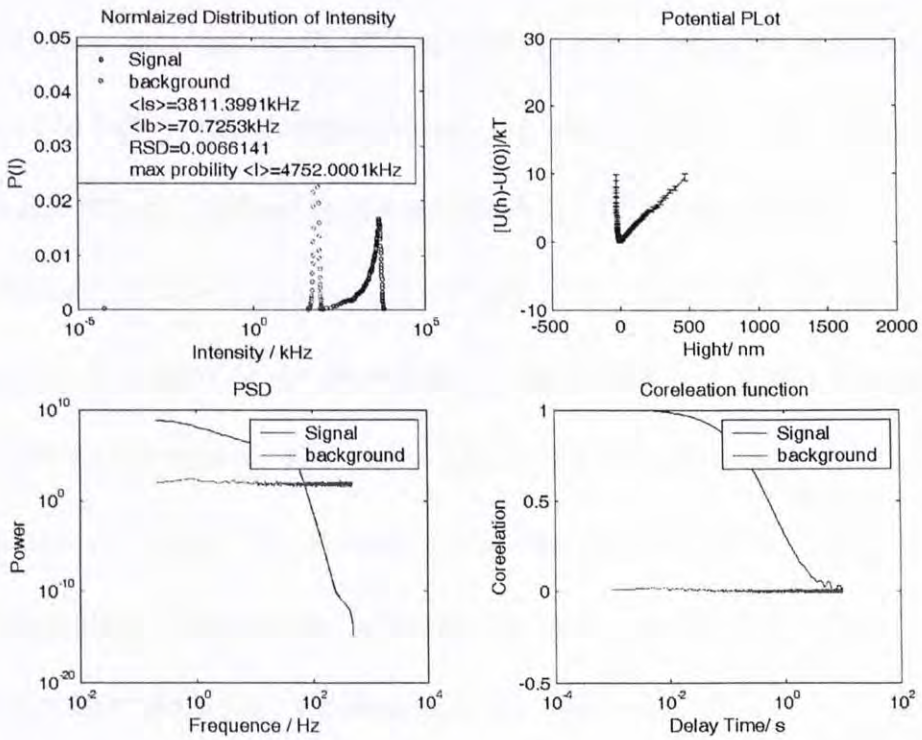

Fig.2-3 Results of our TIRM data analysis with PS 6μm in 0.5mM NaCl.

2.3 Instrumentation

2.3.1 Apparatus

Fig.2-4(a) schematically shows our TIRM setup. The apparatus was mounted on a research graded optical table (M-RS2000-46-8, PL-2000-428, Newport) to reduce the vibrations. The laser beam (maximum=35mW HeNe, λ=632.8nm, TEM_{00} mode, linear polarized, 1145P, JDSU) enters a glass prism (base angle 70.0°; n = 1.51, BK-7 glass; Newport) and is reflected at the bottom side of the sample cell (Premium Slide 75mm×25mm; Fisher Scientific Co.). Because the angle of light incident is larger than θ_c, a total internal reflection results with the generated evanescent wave passing through the interface. The scattered evanescent wave by the selected micro-particle is then collected via the objective (N PLAN, 50x/0.50, WD=7mm, Leica) of the microscope (Leica DM LFSA with electronic focus). The particle is centred on the measuring area (diameter 100 μm), defined by a size-variable iris before the tube lens. The laser beam was focused (Width~20 μm, Length~100 μm in eyepieces after reflection) by lens and directed to the centre of the measurement area by carefully adjusting the metric stages (M-UMR8.25, Newport). The scatted light passes through a beamsplitter (70%R/30%T, Edmund), in where 70% is reflected to the photomultiplier (PMT, H7155 Photo Counting Head, Hamamatsu) while 30% is transmitted to enter the charge coupled device (CCD, Qimaging MicroPublisher 3.3 MC cooled color) for synchronous visual monitoring. A long-wave pass filter (central wave length = 633nm, 10LWF-600-B, Newport) was placed in front of the PMT detector to reduce the background noise.

The sample cell (Fig.2-5) is constructed in house and the sample solution is sandwiched between two glass slides (Premium Microscope Slide, Fisher). The sample solution containing latex particles (typically 3-10μm in diameter) is introduced through two shape needle (diameter = 0.7mm). To the lower glass slide, a special-designed prism is attached to allow the total reflection of laser beam. The two slides are held approximately 1mm apart using an O-ring as a spacer. The sandwiched slides is compressed and mounted tightly by two outer copper blocks with O-ring at contact surface to form a close system. The sample cell is mounted on a mechanic arm which is fixed on a micrometer stage combination with a three-dimension variation (travel stage with dual axis M-406, lab jack 271, Newport). The introduction of the sample solution is through two needles via PTFE tubing by a circulation pump (77912-07 Masterflex, L/S, PTFE-tubing pump system, Cole-Palmer). PTFE tubing is used to avoid interactions between tubing material and sample. Fig.2-4(b) shows a front view of the TIRM. All items are firmly fixed on the optical table.

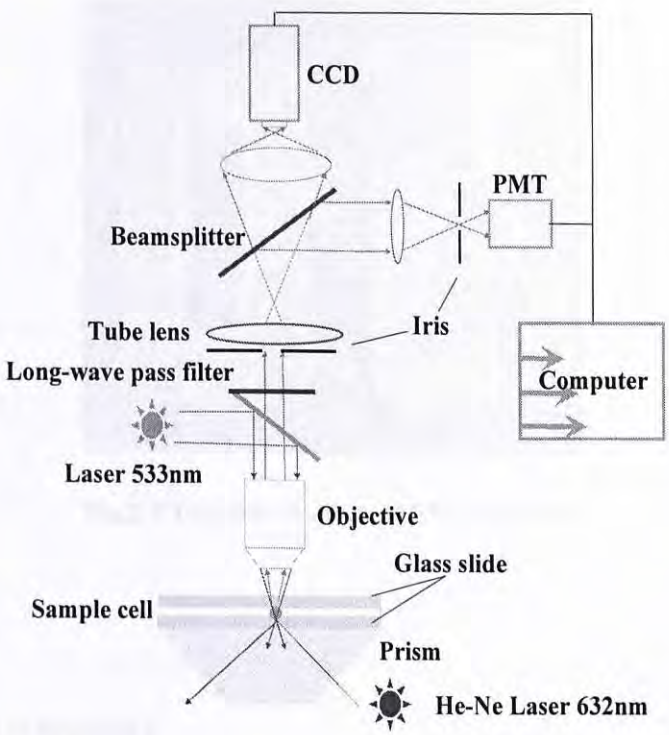

Fig.2-4(a) A schematic diagram of the TIRM.

Fig.2-4(b) Front view of the TIRM setup.

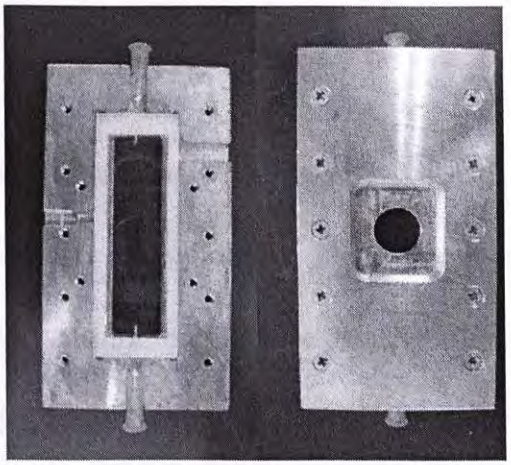

Fig.2-5 The outlook of the TIRM sample cell.

2.3.2 Optical Tweezer

In Fig.2-4(a), a compact solid state laser (maximum output = 400mW, λ = 532nm, DPSS532-400, Coherent#Compass) generates a two-dimensional optical trap after passing through the objective. The trap is strong enough to keep the sphere in place during the solvent exchange and to limit diffusion of the particle parallel to the reflecting plane. The laser source is positioned at the backside of the microscope body. The beam is levitated and introduced into the microscope after passing through a variable neutral density filter (circular variable metallic neutral density, OD range: 0.05-2, 50G02AV.1, Newport) and a beam expander (2-8X, 532nm entrance 8mm, Newport). The expanded beam is then focused by the objective onto the particle. The focus area is around 10 μm from CCD observation. The radiation of the optical tweezer scattered into the PMT is almost totally removed by a long-wave pass filter (Transmission wave length > 600nm, Leica) embedded in the microscope.

2.3.3 Cleaning of the Slide Surface

In our experiments, we used the so called chemical etching method to clean the bottom slide [5,6]. The details are as follows. First, the slides are ultrasonicated with deionized (D.I.) water and ethanol for 15min, separately. Then, the sonicated slides are dipped momentarily in 5% hydrofluoric acid (HF) solution for 5 min. After that, they are rinsed copiously with D.I. water, and stored under the protection in ethanol. Before the TIRM measurement, the slides were dried in pure nitrogen gas and further cleaned by ultraviolet (UV)-ozone plasma cleaner (Harrick Sci. Corp.) for around 5min. This treatment resulted in a reproducible oxide surface, which will be suitable for adsorption studies of nonpolar polymers. Granick et.al. [6-9] has shown that polymers, such as poly(methylmethacrylate) (PMMA), poly(1,4 vinly)pyridine (PVP) can be reproducibly absorbed to the cleaned surfaces.

2.3.4 A Typical Potential Energy Profile

When the separation distance between the particle and surface is several Debye lengths, we can safely expect that Van Der Waals attraction is severely retarded or screened and double-layer repulsion can be well modelled using linear superposition and Derjaguin's approximations. Then for a 1:1 electrolyte, like NaCl aqueous solution, the total potential energy is expected to obey

$$\Phi(h) = B\exp(-\kappa h) + Gh \tag{2.16}$$

where

$$B = 16\varepsilon a\left(\frac{kT}{e}\right)^2 \tanh\left(\frac{e\psi_1}{4kT}\right)\tanh\left(\frac{e\psi_2}{4kT}\right) \tag{2.17}$$

ε is the dielectric permittivity of water, a is the radius of the sphere, e is the elemental charge, ψ_1 and ψ_2 are the Stern potentials of the sphere and the interface,

$$\kappa = \sqrt{\frac{8\pi Ce^2}{\varepsilon kT}} \tag{2.18}$$

is the Debye parameter, C is the total ionic strength, and

$$G = \frac{4}{3}\pi a^3(\rho_s - \rho_f)g \tag{2.19}$$

is the net weight of the sphere. Eq.2.16 has a single minimum at

$$\kappa h_m = \ln\frac{\kappa B}{G} \tag{2.20}$$

The charge parameter B is difficult to determine independently. Fortunately, we can eliminate B between Eq.2.16 and 2.18 to obtain the relative potential energy in terms of the relative separation distance h - h_m:

$$\frac{\Phi(h)-\Phi(h_m)}{kT} = \frac{G}{\kappa kT}\left\{\exp\left[-\kappa(h-h_m)\right]-1\right\}+\frac{G}{kT}(h-h_m) \tag{2.21}$$

In other words, the shape of the potential energy profile is not affected by B. Increasing the charge on either the sphere or the interface will shift the minimum to larger

separation distances h_m according to eq(1.20), but it does not affect the shape of the profile. Fig.2-6 shows a typical interaction potential between a charge polystyrene sphere and a charge surface, in which only gravity and double-layer repulsion are dominated.

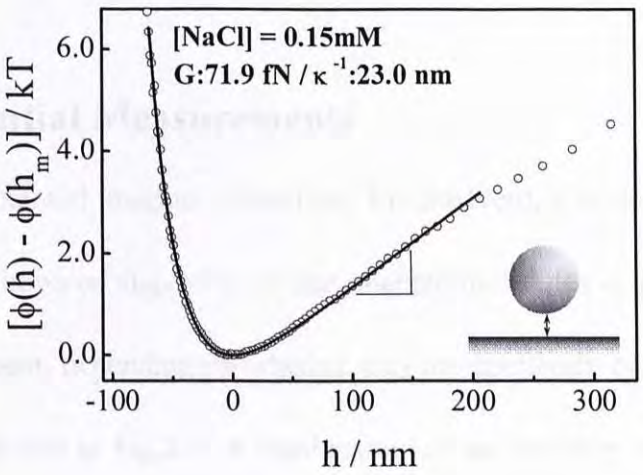

Fig.2-6 Potential profile of PS (diameter 6μm) in 0.15mM NaCl aqueous solution. The solid curve is equation (15) with G:71.9*f*N, κ^{-1}:23.0nm.

2.4 Laser light scattering (LLS)

In a typical experiment, a laser light beam impinges on a solution and is scattered into a photomultiplier tube placed at an angle with respect to the transmitted beam. In static LLS, the measurements of the angular and concentration dependence of the absolute time-average scattered intensity can lead to the weight-average molar mass, the radius of gyration, and the second virial coefficient of polymer chains in solution. In dynamic LLS, a spectral broadening of the light scattered from polymer chains will be observed. For a pure diffusive relaxation, the observed line-width in a dilute solution can

be related to the translational diffusion or the hydrodynamic size of polymer chains. This spectral broadening can be effectively recorded in the form of a time correlation function through a digital time correlator [15]. A combination of static and dynamic LLS results can monitor the conformation change of polymer chains.

2.5 Zeta-potential Measurements

In the Zeta-potential analyzer (Zeta-Plus, Brookhaven), a static electrical field will be applied in a solution or dispersion so that charged molecules or particles will have a directional movement, depending on whether they are positively or negatively charged. The set up have shown in Fig.2-7. A combination of the mobility and particle size can lead to an average surface charge density, often expressed as the zeta-potential. The zeta-potential, ξ, is normally calculated from the electrophoretic mobility (μ) using the Smoluchowski relationship, $\xi = \eta\mu/\varepsilon$, where it is assumed that $\kappa a >> 1$, where η is the solution viscosity, ε is the dielectric constant of the medium, κ and a are the Debye-Huckel parameter and the particle radius, respectively.

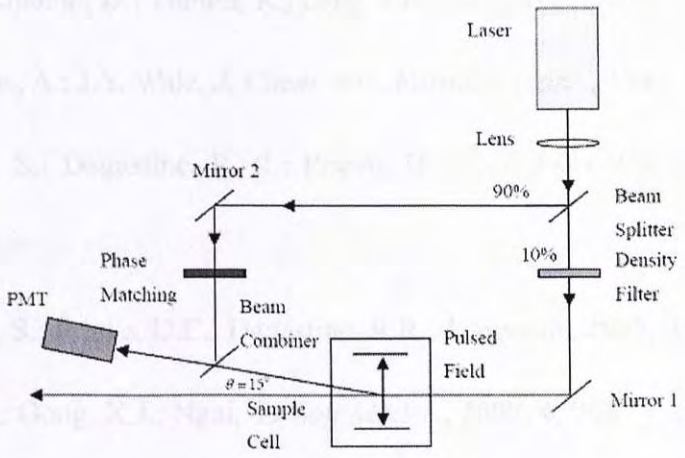

Fig.2-7 Set up of Zeta-Plus

2.6 References and Notes

1. Prieve, D.C; Luo, F.; Lanni, F., *Faraday Discuss.Chem.Soc.,* **1987**, 83, 297.

2. Helden, L.; Roth, R.; Koenderink, G.H.; Leiderer, P.; Bechinger, C., *Phys. Rev. Lett.*, **2003**, 90, 48301.

3. Rudhardt, D.; Bechinger, C.; Leiderer, P., *Phys. Rev. Lett.*, **1998**, 81, 1330.

4. Kleshchanok, D.; Tuinier, R.; Lang, P.R., *Langmuir*, **2006**, 22, 9121.

5. Sharma, A.; J.Y. Walz, *J. Chem. Soc. Faraday Trans.*, **1996**, 92, 4997.

6. Biggs, S.; Dagastine, R. R.; Prieve, D. C., *J. Phys. Chem.*, **2002**, 106, 11557.

7. Biggs, S.; Prieve, D.C.; Dagastine, R.R., *Langmuir*, **2005**, 21, 5421.

8. Jin, F.; Gong, X.J.; Ngai, T., *Soft Matter.*, **2008**, 4, 968.

9. Bevan, M.A.; Prieve, D.C., *Langmuir*, **2000**, 16, 9274.

10. Fernandes, G.E.; Bevan, M.A. *Langmuir*, **2007**, 23, 1500.

11. Kleshchanok, D.; Lang, P.R., *Langmuir* ,**2007**, 23, 4332.

12. Bevan, M.A.; Prieve, D.C., *Langmuir*, **1999**, 15, 7925.

13. Chew, H.; Wang, D.S.; Kerker, M., *Appl. Opt.*, **1979**, 18, 2679.

14. Flicker, S.G.; Bike, S.G., *Langmuir*, **1993**, 9, 257.

15 Chu, B., *Laser Light Scattering: Basic Principles and Practice* Academic Press: Boston, 1991.

Chapter 3

Depletion Attraction between a Polystyrene Particle and a Hydrophilic Surface in a Pluronic Aqueous Solution

3.1 Introduction

The application of colloidal particles in many industries is often intimately connected to the use of polymers. Examples include cosmetics, water treatment, foodstuffs, paints, and inks, to mention but a few [1]. Polymers may be adsorbed to the particles, chemically attached to their surfaces or they may be free in solution. Whichever form they take, their presence has a major effect on both the stability and viscosity of colloidal dispersions. As a result, the study of colloid-polymer mixture is an area of active research directly of interest to many industries [2,3].

To understand the effect of an additional polymer on colloidal interaction, the basic question is whether the polymer adsorbs at the particle surface or not. To act as stabilizers, polymers must adsorb or graft onto the surface of the particle which can lead to a steric or electrosteric repulsion. Under certain circumstances, however, high molecular weight polymers can adsorb on separate particles and draw them together, a phenomenon known as polymer bridging [1,4]. In practice, the steric or electrosteric stabilization of colloidal particle are majority imparted by copolymers, but more often

by specifically block copolymers. In these cases, one block of the copolymer is designed preferentially to strongly interact with the surface of the particle; while the other block is designed not to adsorb onto the surface of particle but just to extend to the solution. The interaction forces depend on the surface coverage, on whether the polymer chains are reversible or irreversible adsorbed, and on the quality of the solvent [5-8].

If the polymer chains do not adsorb onto the surfaces, an attractive depletion force between the dispersed particles will occur at low polymer concentration. Asakura and Oosawa were the first to describe this force and its origins [9]. Qualitatively it can be understood by considering of two large particles in a solution consisting of nonadsorbing polymers, then for large surface separations the polymer concentration in the region between the particles will essentially be the same as for the bulk solution. However, if the interparticle separation is reduced to a value less than the characteristic size of polymer in solution, then any polymer molecules entering the gap between the particles will have a reduced configurational entropy, since the total number of possible conformations of such chains is now reduced. As a result, polymer will be excluded from the gap, leading to a local region between the particles which is solvent-rich. Solvent molecules will tend to move out of the gap region into the bulk, effectively "pulling" the two particles together, giving rise to the so-called depletion attraction effect. The magnitude of this depletion attraction is proportional to the osmotic pressure difference between the interparticle gap region and the bulk solution [10]. Depletion forces have been measured in the presence of nonadsorbing nanoparticle suspensions [11], surfactant micellar solutions [12,13], polymer solutions [14,15] and in charged

polyelectrolytes [16,17]. The studies have confirmed the main features of the expected depletion interaction.

It should be mentioned that among different commercially available block copolymers, Pluronic triblock copolymer is the one of the most widely used industrial stabilizers. The Pluronics are of the form PEO_n-PPO_m-PEO_n; where PEO is poly(ethylene oxide) and PPO is poly(propylene oxide). The usefulness of the Pluronics comes from the differing solubilities of the PEO and PPO blocks. The PPO blocks, which are hydrophobic and expect to adsorb at interface particularly when the interface is hydrophobic; on the other hand, the hydrophilic PEO are though to extend into the aqueous phase to provide a steric repulsion of the dispersed particles. Numerous studies have been performed to investigate the Pluronic copolymers both in solution and adsorption onto colloidal particles [18-23]. In addition, some of the studies mentioned above have also considered the biocompatibility of adsorbed layers containing Pluronic molecules. For example, Tan et al. [20] have shown that the lifetime of polystyrene latex particles injected into the bloodstream of rabbits and rats could be significantly increased by coating them with Pluronic triblock copolymers.

Several groups have also direct measured interparticle forces between surfaces bearing adsorbed Pluronic triblock copolymers. In general, the interaction forces between colloidal particles are weak, within several kT. The direct measurements have only recently become possible with the improved sensitivity afforded by techniques such as surface force apparatus (SFA) [24,25] optical tweezers [26], atomic force

microscopy (AFM) [27-29], and total internal reflection microscopy (TIRM) [30-32]. For example, using AFM, both Musoke et al. [27] and McLean et al. [28] found that the interaction forces obtained between Pluronic triblock copolymer layers adsorbed onto hydrophobic surface in a high ionic strength aqueous solution were repulsive in nature due to the steric overlap between the adsorbed polymer layers. Bevan and co-workers [30-31] have used the technique of TIRM to monitor the interactions between polystyrene latex particles and a flat surface bearing adsorbed Pluronic copolymers. The steric repulsion was also observed in their studies which appeared as a virtual "hard wall" repulsion. In recent studies, Tulpar et al. [29] have measured interparticle forces between surfaces in mixed Pluronic-surfactant systems. They found that surfactant caused the Pluronic copolymer to extend, forming relatively large, charged complexes that generated a significant depletion forces between the particle and surface plate.

In this chapter, we present the results of using TIRM to directly measure the interactions between a 6.0 μm polystyrene sphere and a hydrophilic silica plate in the presence of PE10500 triblock copolymer aqueous solution. In contrast to the earlier studies, we performed the force measurements in a low ionic strength aqueous condition so that the separation distance between the bare particle and surface was reduced to around 133 nm. We found that in such low salt concentration, monomer, micelles and larger nanobubbles coexist when PE10500 solution was spontaneously dissolved. Most significantly, the existence of these nanobubbles can induce a depletion attraction pushing the spherical particle close to the flat hydrophilic surface. As expected, both the magnitude and range of the depletion attraction is salt concentration dependent.

3.2 Experimental Section

3.2.1 Sample Preparation

Polystyrene sulfonate latex particles with a diameter of ~6.0 μm (CV 4.1%) were purchased from Interfacial Dynamics Co., U.S.A. and used without further treatment. Silica microscopy slides (BK-7 glass, Fischer Scientific Co.) were first thoroughly cleaned by ultrasonication 15 mins in ethanol, and then dried by blowing with highly pure nitrogen. After that, the dried slides were dipped in 5% HF solution and then washed with deionized water again. The treated slides were kept in ethanol and further cleaned by UV-zone plasma cleaner (Harrick Sci. Co.) before assembling the sample cell. Pluronic PE10500 triblock copolymer (PEO_{37}-PPO_{56}-PEO_{37}, total molecular weight, ~6,500 g/mol) was a gift from BASF Corp. and used without further purification. In this work, all PE10500 triblock copolymer solutions with concentration of 5.0×10^{-3} g/mL were prepared at a background concentration of 0.2 mM, 0.5 mM and 1.0 mM sodium chloride (NaCl) respectively. No pH adjustment was made. The NaCl (GR from BDH) was heated at ~200 °C for ~2 days to remove organic impurities. Water was purified with an inverse osmosis filtration (Nano Pure, Barnstead) until its resistivity reached 18.2 MΩ•cm at 20 °C and then filtered with a Milipore PTFE 0.45-μm hydrophilic filter.

3.2.2 Total Internal Reflection of Microscopy

The interaction potential profiles between a single polystyrene (PS) particle and the hydrophilic silica surface in the presence of polymer solutions were determined by TIRM. Details about TIRM has described in chapter 2.

Typically, we first measured the potential energy between a PS particle and a hydrophilic glass surface in pure NaCl solution with the concentration of 0.2mM. After that, PE10500 triblock copolymer solutions (C = 1.5×10^{-3} g/mL) spontaneously dissolved in desired NaCl concentrations were introduced in sample cell to replace the pure NaCl solution by a flex tubing pump (Master Flex), while the PS particle was trapped in place by tweezers. At least ~20 mL of fluid was used to change solutions (changing the volume inside the sample cell at least 10 times). After completely replacement and waited for 12 hrs, the interaction potentials between the PS particle and the surface in the presence of PE10500 copolymer solution were measured. In the next step, the particle was trapped again and the sample cell was rinsed with a large amount of salt solution. The interaction between PS particle and surface was measured after the salt rinsing. Note that in this manner, we can exchange the solution inside the sample cell between the salt solution and PE10500 copolymer solution repeatedly, but keep using the same particle and glass slide which can significantly reduce the effects of particle and surface variations.

The last portion of this experiment is the distance calibration of the height between particle-surface where a high concentration of salt solution (100 mM) was pumped in to

screen the repulsion levitating the PS particle. The particle will then "stuck" to the plate and the scattering intensity was measured. A region where there are no particles in the microscopy field was then selected to determine the background scattering intensity. The difference between the average of the "stuck" particle intensity and the average of the background intensity is taken to be I_0 in Eq. 3.1 [33]

3.2.3 Laser Light Scattering

A modified commercial light-scattering spectrometer equipped with an ALV-5000 multi-τ digital time correlator and a He-Ne laser (output power =22 mW at λ_0 = 632nm) was used. The measurable angular range is 15-155°. The details of the LLS instrumentation and theory can be found elsewhere [34,35]. The PE10500 triblock copolymer solution used in this study was prepared by spontaneously dissolving PE10500 in desired NaCl salt solution (C = 5.0 × 10^{-3} g/mL) at ~25 °C. No pH adjustment was made. In dynamic laser light scattering (DLS), the intensity-intensity time correlation function $G^{(2)}(\tau)$ in the self-beating mode was measured in the scattering angle range 17.5°-150°. The Laplace inversion of $G^{(2)}(\tau)$ can lead to a line-width distribution $G(\Gamma)$, which can be further converted to a translational diffusive coefficient distribution $G(D)$ by $\Gamma=Dq^2$ or a hydrodynamic radius distribution $f(R_h)$ by use of the Stokes-Einstein equation, $R_h = k_B T / 6\pi\eta D$, where η, k_B, and T are the solvent viscosity, the Boltzmann constant, and the absolute temperature, respectively. Moreover, in some case, the electrophoretic mobility of the PE10500 copolymer in aqueous solution was

measured using a commercial zeta-potential spectrometer (ZetaPlus, Brookhaven).

3.3 Results and Discussion

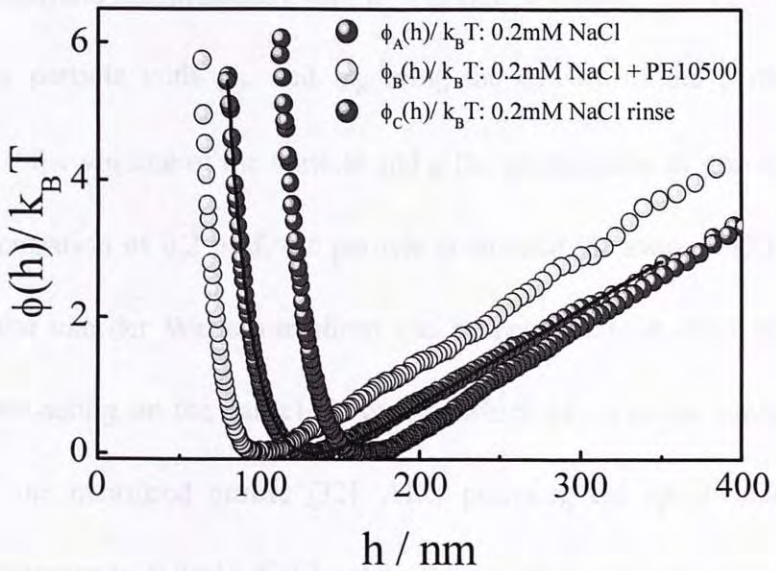

Fig.3-1 The measured interaction potentials (ϕ (h)/k_BT) between a PS particle and a glass surface under different condition. ϕ_A(h)/k_BT: the interaction potential between the bare PS particle and surface in 0.2 mM NaCl solution; ϕ_B(h)/k_BT: the interaction potential between the PS particle and surface after pumping the spontaneously dissolved PE10500 triblock copolymer in 0.2 mM NaCl solution; ϕ_C(h)/k_BT: the interaction potential between the PS particle and surface after rinse with 0.2 mM NaCl solution. The solid line is a theoretical fitted curve from Eq.3.

Fig.3-1 shows that in the absence of PE10500 triblock copolymer, there are just two contributions to the interactions between the PS particle and flat surface in 0.2 mM NaCl aqueous solution; namely, the electrostatic double layer repulsion on the left side

of the minimum and gravitational energy on the right side of the minimum, which can be described by the following equation [32,33]:

$$\frac{\phi(h)}{k_B T} = Be^{-\kappa h} + \frac{G}{k_B T}h \tag{3.1}$$

where B is a function of the surface potential between the surface and particle, which is difficult to determine independently and κ^{-1} is Debye length. $G(=(\rho_P - \rho_W)Vg)$ is the weight of the particle with ρ_P and ρ_W being the density of the particle and water respectively, V the volume of the particle and g the acceleration of gravity. Note that at the salt concentration of 0.2 mM, the particle is situated far away (~133 nm) from the surface that the van der Waals attractions can be neglected. In other words, the only attractive force acting on the particle is gravity which gives to the straight line on the right side of the measured profile [32]. After pumping the spontaneously dissolved PE10500 copolymer in 0.2mM NaCl solution through the sample cell and waited for ~12 hrs, Fig.3-1 clearly shows that the measured potential profile became deeper and shifted closer to the flat surface, indicating that the addition of PE10500 copolymer solution has induced an attraction. However, after rinsing the sample cell again with 0.2mM NaCl solution, the measured potential profile moved to larger separation. In other words, the induced attractive force disappears.

It is expected that when PE10500 triblock copolymer solution is pumped into the sample cell, they will be adsorbed onto both the PS particle and silica surface, especially to the surface of PS which is hydrophobic in nature. McLean et al. [28]

showed that the PEO-PPO-PEO triblock copolymers can absorb onto hydrophobic surface with the PEO chains extend normal to the surface forming a brush layer, whereas at the hydrophilic silica surface, they exist as noninteracting, isolated polymeric mushrooms. It is worth noting that several groups have also directly measured interparticle forces between surfaces containing layers of adsorbed PEO-PPO-PEO block copolymers. For example, by applying AFM [28,29] and TIRM [30] techniques, the reported interaction forces between surfaces in the presence of PEO-PPO-PEO triblock copolymer layers were the expected purely repulsive force, rather than attractive in nature. In comparison to these studies, the only apparent difference in our experiments and those mentioned studies is that our force measurements were done in a low ionic strength aqueous solutions, while the reported measurements [28-30] were performed in a relatively high ionic strength (≥100 mM) aqueous solutions. In this way, the electrostatic repulsion between the charged particle and surface in such high ionic strength solution will be sufficiently suppressed; leaving solely the steric repulsion can be detected. Then, what is the nature of our measured long-range attraction with the presence of PE10500 copolymer in the low ionic strength aqueous solution? We will come back to this point later.

Since we have used the same particle and the hydrophilic silica surface to obtain a complete set of interaction potential profiles shown in Fig.3-1 (the details has been described in experimental part), it enables us to compare the measured potential profiles even they were under different conditions. Moreover, in order to isolate the effects of the adsorbed PE10500 copolymer onto both particle and flat surface, we take the

difference of the measured potentials before ($\phi_B(h)/k_BT$) and after ($\phi_C(h)/k_BT$) rinsing with the salt solution. We believe that rinsing the sample cell with salt solution is rather difficult to desorb the adsorbed PE10500 copolymer chains completely. Qualitatively this can be understood by considering that for each adsorbing site (which could involve a small segment of the chain), there exists a dynamic equilibrium between the adsorption and desorption. However, a complete desorption of a PE10500 chain from the surface requires not only a simultaneously releasing of all the adsorbing sites but also the fast diffusion of the chain away from the surface. Therefore, it is rather difficult for an adsorbed PE10500 chain to become free again after its adsorption on the surface [36]. Fig.3-2 shows the result of such subtraction. It clearly shows that there has an attraction ($\phi_{Dep}(h)/k_BT$), which is continuous and with the measurable distance up to ~100 nm. The measured attraction is not van der Waals attraction since it arises at a much greater distance. One therefore may conjecture that this attraction could be due either to a depletion effect or to polymer bridging in the presence of PE10500 copolymer. To test our hypothesis, we first used DLS to study the PE10500 triblock copolymer in the low ionic strength aqueous solution.

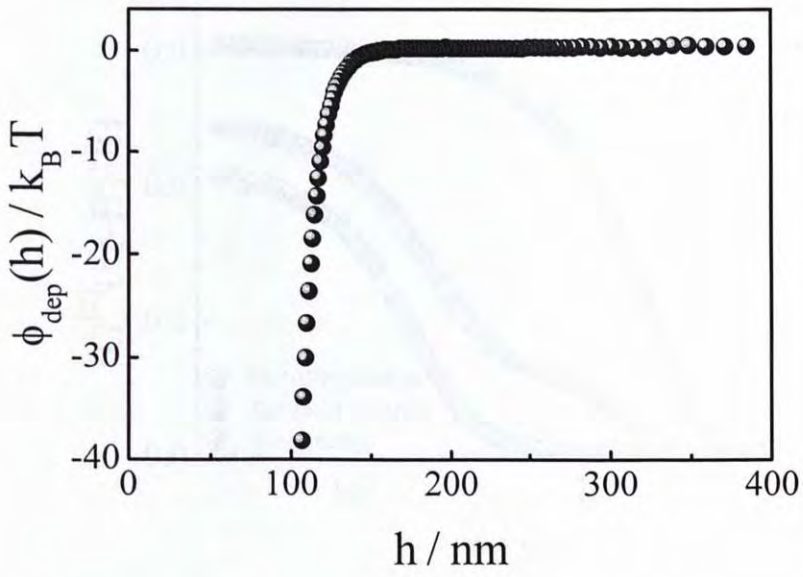

Fig.3-2 Measured depletion potential ($\phi_{Dep}(h) = \phi_C(h) - \phi_B(h)$) between a PS particle and a glass surface with the presence of charged bulk-free nanobubbles.

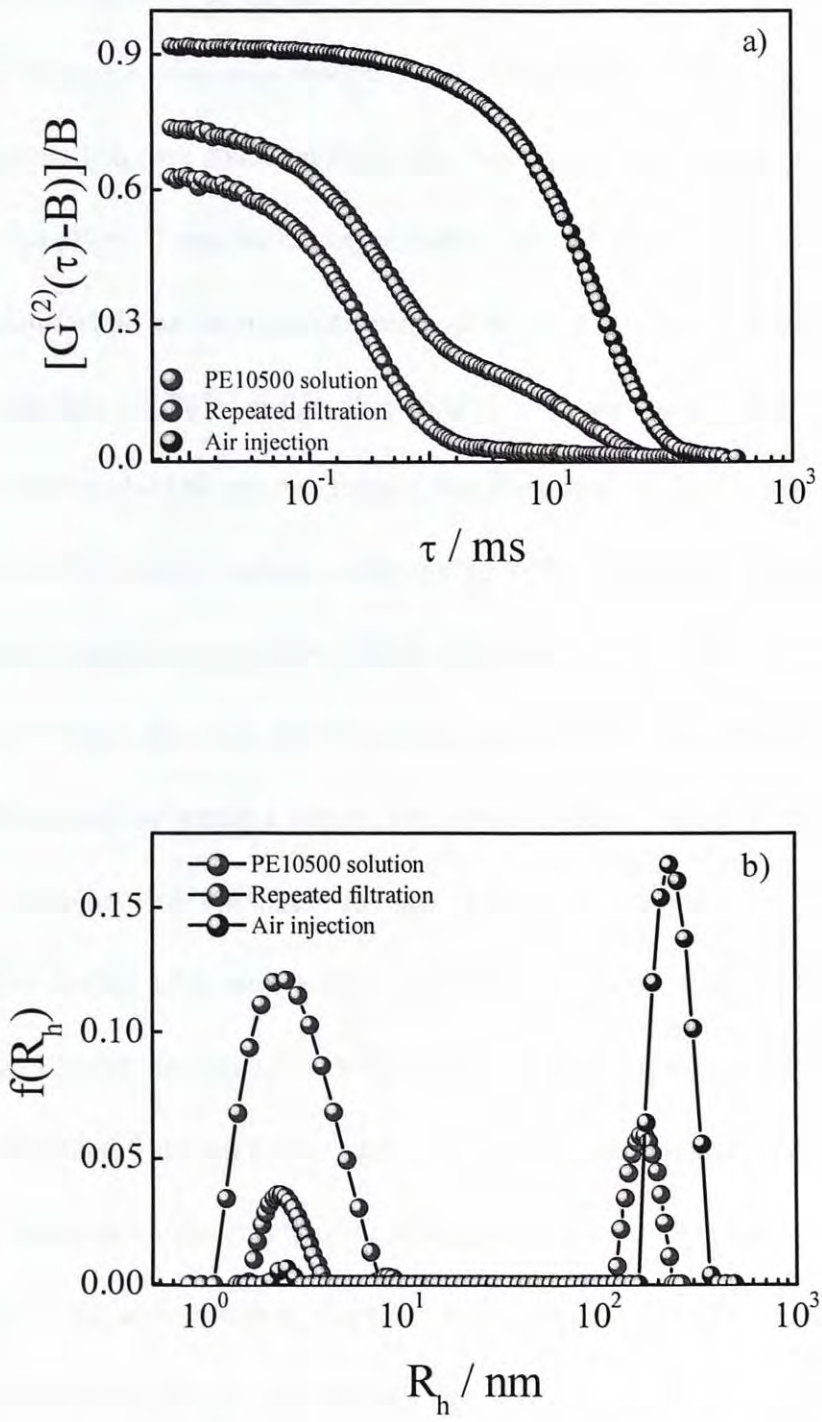

Fig.3-3 Normalized intensity-intensity time correlation functions ($[G^{(2)}(\tau)-B] / B$) and their corresponding average hydrodynamic radius ($<R_h>$) of PE10500 triblock copolymer in 0.2 mM NaCl solution before and after 200-times filtration as well as directly air injection.

Fig.3-3(a) shows that the measured normalized intensity-intensity time correlation functions ($[G^{(2)}(\tau) - B] / B$) of PE10500 triblock copolymer in 0.2mM NaCl solution contains more than one relaxation modes. The corresponding average hydrodynamic radius distributions $f(R_h)$ are shown in Fig.3-3(b). The average hydrodynamic radius of the fast mode is only ~2.7 nm, attributing to individual PE10500 molecules free in the aqueous solution, while an intermediate peak of about ~ 7.0 nm is evident for the formation of micelles [37,38]. On the other hand, for the slow mode with an average hydrodynamic radius of ~166 nm, we suggest that they may be due to relatively large nanobubbles free in aqueous solution, but not to some previously suggested large "clusters" made of micelle aggregation. [37,38] The first direct evident comes from the fact that the slow mode shown in Fig.3-3(a) can be completely removed after repeated filtration (~200-times) by using a tubing flex pump (Master Flex). In the repeated filtration, the solution was circulated to pass through a Millipore 0.45 μm PTFE hydrophilic filter and the LLS cuvette in a closed loop that the filtration has no effect on the PE10500 copolymer concentration as PE10500 is a small molecule. It should be also stated that the repeated filtration has no significant effect on the fast mode, and the slow mode did not reappear in the solution for a long time after its removal as shown in Fig.3-3(a) and 3-3(b). In other words, the solutions were very stable. In the second step, which we think is crucially important. Namely, we found that gently injecting dust-free air into slow-mode-free solution can bring the slow relaxation mode back, as shown in both Fig.3-3(a) and 3-3(b). The peak related to such reappearing slow mode is generally larger and broader than those spontaneously dissolved PE10500 solution because we

injected air inside. Note that in recent studies, Jin et al. [39-41] have also confirmed that the formation of nanobubbles is actually a very common phenomenon in many aqueous solutions containing of water-soluble organic molecules, in particular for some surfactant/water systems. As a consequence, we suggest that the slow mode observed in the spontaneously dissolved PE10500 copolymer solution in 0.2mM NaCl solution is related to small bubbles. Presumably, the stabilization of these nanobubbles free in solution can be attributed to a preferential adsorption of small amphiphilic PE10500 triblock copolymer at the gas/water interface. On the other hand, it is worth noting that $f(R_h)$ shown in Fig.3-3(b) is an intensity-weight distribution and that large bubbles scatter much more light than individual PE10500 chains and micelles, particularly measured at a smaller scattering angle ($\theta = 20.0°$). Therefore, the position of the peak located at ~166 nm actually represents only a very small number of nanobubbles free in solution even if its area looks large. Furthermore, the electrophoretic mobility of the bulk-free nanobubbles was found to be $\mu_E \sim -1.13 \times 10^{-8}$ $m^2/s \cdot V$, indicating that the nanobubbles are negatively charged. This probably can be related to the adsorption of OH^- ions to the interface from the dissociation/association of water, which is consistent with other studies. [40]

Having an overview of experimental evidence for the existence of bulk-free nanobubbles by spontaneously dissolved PE10500 copolymer in the low ionic strength aqueous solution, and demonstrated that they can be deliberately removed by repeated filtration and regenerated by air injection, we can now discuss the effects of presence or absence of these bulk-free nanobubbles on the interaction between the PS particle and

flat surface as shown in Fig.3-1. As the nanobubbles free in PE10500 aqueous solution have just been shown to be negatively charged and we have used sulfonated PS particle and the hydrophilic glass surface (both are negatively charged) in the TIRM measurements, we can reasonably assume that charged nanobubbles will not preferentially absorb to both the particle and glass surface. In this way, we conjecture that the measured attraction shown in Fig.3-1 and 3-2 may be the depletion attraction caused by the exclusion or depletion the large charged nanobubbles from the gap between the PS particle and glass surface as the separation distance between the particle-surface (~133 nm) is smaller than the physical size of the charged nanobubbles (~166 nm) under the condition of 0.2 mM NaCl aqueous solution. We applied a classical depletion potential function to fit the measured profiles shown in Fig.3-2, namely

$$\begin{aligned} \phi_{dep}(h) &= -\pi\Pi[(a+\Delta)(h-2\Delta)^2 + \frac{1}{3}(h-2\Delta)^3] \quad for \quad 0 < h < 2\Delta \\ &= 0 \qquad\qquad\qquad\qquad\qquad\qquad\qquad\qquad for \quad h > 2\Delta \end{aligned} \tag{3.2}$$

where Π is the osmotic pressure of the bulk solution, a is the radius of the PS particle (here a = 3.0 μm) and 2Δ is the depletion region [42,43]. The fitting gives the depletion region (2Δ) and osmotic pressure (Π) as 140.0 nm and 14.5 Pa, respectively. The relatively larger Π may be due to the "charged" nanobubbles. It has been shown that for the same molar concentration, charged species can have much larger osmotic pressures than neutral depletants because electroneutrality requires the counterions to remain with them, each counterion can then contribute as much to the osmotic pressure

as each non-charged depletants [42,43].

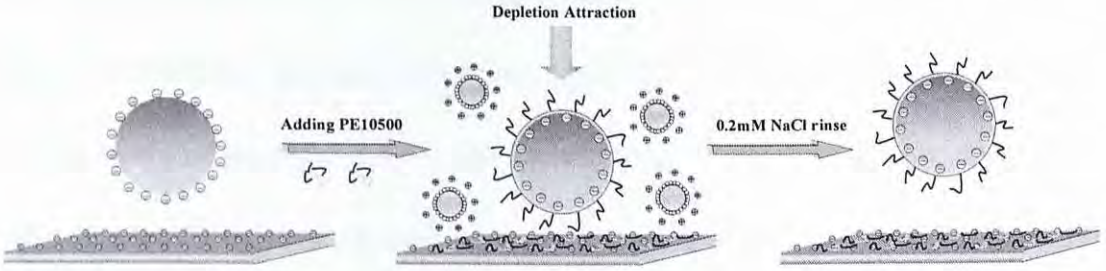

Fig.3-4 Schematic shows the depletion attraction induced by some charge nanobubbles in the spontaneously dissolved PE10500 in 0.2 mM NaCl aqueous solution as well as the effect of interaction between the PS particle and surface after rinse with 0.2 mM NaCl solution. "-" present negatively charge, "+" present counterion (not in a proportional scale).

Fig.3-4 has schematically shown the effects of pumping PE10500 triblock copolymer aqueous solution on the interaction between the spherical PS particle and flat hydrophilic surface. The formation of stable nanobubbles in the low ionic strength aqueous solution of PE10500 triblock copolymer is a spontaneous process. The existence of these nanobubbles can induce an attraction between the particle and surface. The origin of such measured attraction is attributed to the depletion of large nanobubbles from the gap between particle and glass surface, resulting in an imbalance osmotic pressure inside and outside the gap. This further leads to a net depletion force acting on the particle so that it moves closer to the flat surface as shown in Fig.3-1. On the other hand, after rinse the sample cell with the salt solution, the net attractive force disappears because the spontaneously generated nanobubbles have been completely removed. However, we believe that rinsing the sample cell is rather difficult for the adsorbed PE10500 chain to become free again as mentioned before. We conjecture that

the adsorption of PE10500 chains at both charged particle and flat surface might cause the redistribution of the counter-ions and co-ions that make up the electric double layer from the surfaces, probably adsorption more ions to the surface and resulting in displacement of the repulsive potential between the particle and surface. This explains why the particle moves even more far away from the surface after rinsing in comparison to the measured interaction potential between bare particle and surface under the same salt concentration as shown in Fig.3-1.

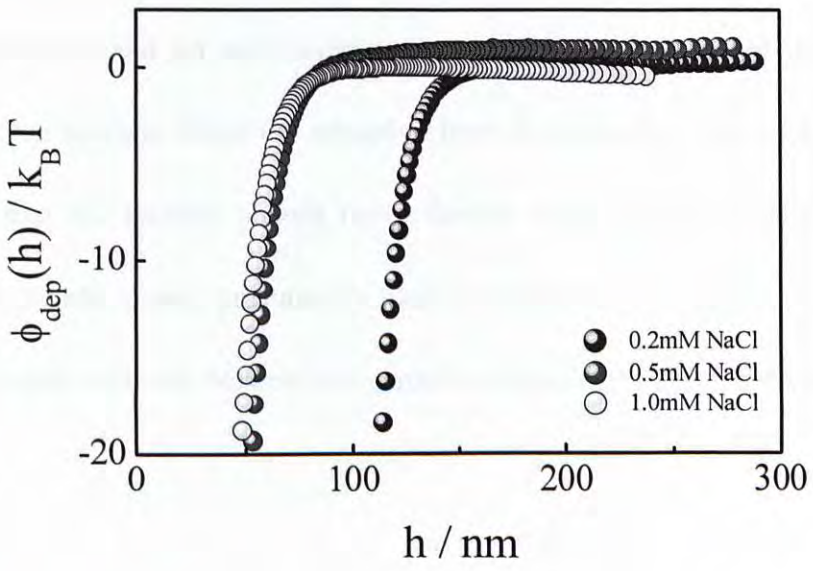

Fig.3-5 The effect of salt concentration on the interaction between PS particle and surface in the PE10500 triblock copolymer aqueous solution.

Fig.3-5 shows that both the magnitude and range of the nanobubble-induced depletion force are reduced with increasing the ionic strength of the solution. The

reduction of magnitude of the depletion force is attributed to the decrease of osmotic pressure difference inside and outside the gap by increasing the electrolyte concentration. The fitting shows that Π decreases from 14.5pa to 6.8pa when salt concentration increases from 0.2mM to 1mM, indicating the suppression of the charges [44.45]. On the other hand, for the reduction in the range of the depletion force, we attribute it to the reduction in the effective size of the charged nanobubbles which arises from the screening of the charge on all surfaces by the electrolyte. Jin et al [41] showed that the addition of salt can even induce the nanobubble aggregation. In addition, we found that the particle moves closer to the surface when the concentration of electrolyte was increased, and for salt concentration was greater than 3 mM, the particle would stick to the surface. Since the attractive force is reduced by the electrolyte, one might expect that the particle should move further away from the surface. However, the particle moves closer, presumably, this movement is due solely to a weakening of double-layer repulsion between the particle and surface with the addition of electrolytes.

3.4 Conclusion

By using a combination of LLS and TIRM measurements, we found that, in the low ionic strength solution, stable nanobubbles can be spontaneously formed in the PEO-PPO-PEO triblock copolymer aqueous solutions, which previously was related to the micelle aggregation. Moreover, the existence of these nanobubbles can induce a depletion attraction between a spherical particle and a flat surface. Using TIRM, we

have directly measured this depletion force with the distance up to ~100 nm. Our results show that the origin of such attraction comes from exclusion or depletion the charged nanobubbles between the gap of particle and flat surface. This results in an imbalance between the osmotic pressures inside and outside the gap and then leads to a net attractive force pushing the particle to the surface. The magnitude and also the range of this depletion force can be tuned by the ionic strength of the solution. By considering that PEO-PPO-PEO is the most commonly used industrial stabilizer, our results thus shed light on the stability of application of colloid-polymer mixtures in the industries.

3.5 References and Notes

1. Napper, D. H. *Polymeric Stabilization of Colloidal Dispersions*, Academci Press: London, **1983**.
2. Farinato, R. S.; Dubin, P. L. eds., *Colloid-Polymer Interactions: From Fundamentals to Practice,* Wiley-VCH, **1999**.
3. Urban, D.; Takamura, K. eds., *Polymer Dispersions and Their Industrial Applications*, Wiley-VCH, **2002**.
4. Swenson, J.; Smalley, M. V.; Hatharasinghe, H. L. M. *Phys. Rev. Lett.* **1998**, 81, 5840.
5. de Gennes, P. G. *Macromolecules* **1982**, 15, 492.
6. Pincus, P. A.; Klein, J. *Macromolecules* **1982**, 15, 1129.
7. Scheutjens, J. M. H. M. G.; Fleer, J. *Macromolecules* **1985**, 18, 1882.
8. Klein, J.; Rossi, J. *Macromolecules* **1998**, 31, 1979.
9. Asakura, S.; Oosawa, F. *J. Chem. Phys.* **1954**, 22, 1255.
1.0 Tuinier, R.; Rieger, J.; de Kruit, C. G. *Adv Colloid Interface Sci.* **2003**, 103, 1.
11. Sharma, A.; Walz, J. Y. *J. Chem. Soc., Faraday Trans.* **1996**, 92, 4997.
12. Richetti, P.; Kekicheff, P. *Phys. Rev. Lett.* **1992**, 68, 1951.
13. Sober, D. L.; Walz, J. Y. *Langmuir* **1995**, 11, 2352.
14. Milling, A.; Kendall, K. *Langmuir* **2000**, 16, 5106.
15. Piech, M.; Walz, J. Y. *J. Phys. Chem. B* **2004**, 108, 9177.

16. Biggs, S.; Dagastine, R. R.; Prieve, D. C. *J. Phys. Chem. B* **2002**, 106, 11557.

17. Biggs, S.; Prieve, D. C.; Dagastine, R. R. *Langmuir* **2005**, 21, 5421.

18. Bahadur, P.; Pandya, K. *Langmuir* **1992**, 8, 2666.

19. Brown, W.; Schillen, K. *J. Phys. Chem.* **1992**, 96, 6038.

20. Tan, J. S.; Butterfield, D. E.; Voycheck, C. L.; Caldwell, K. D.; Li, J. T. *Biomaterials* **1993**, 14, 823.

21. Li, J. Q.; Caldwell, K. D. *Colloids Surf., B* **1996**, 7, 9.

22. O'Connor, S. M.; DeAnglis, A. P.; Gehrke, S. H.; Retzinger, G. S. *Biotechnol. Appl. Biochem.* **2000**, 31, 185.

23. Bogber, M.; Ring, T. A.; Caldwell, K. D. *Macromolecules* **2002**, 35, 6724.

24. Ruths, M.; Yoshizawa, H.; Fetters, L. J.; Israelachvili, J. N. *Macromolecules* **1996**, 29, 7193.

25. Moore, N. M.; Kuhl, T. L.; *Langmuir* **2006**, 22, 8485.

26. Verma, R.; Crocker, J. C.; Lubensky, T. C.; Yodh, A. G. *Macromolecules* **2000**, 33, 177.

27. Musoke, M.; Luckham, P. F. *J. Colloid Interface Sci.* **2004**, 277, 62.

28. McLean, S. C.; Lioe, H.; Meagher, L.; Craig, V. S. J.; Gee, M. L. *Langmuir* **2005**, 21, 2199.

29. Tulpar, A.; Tilton, R. D.; Walz, J. Y. *Langmuir*, **2007**, 23, 4351.

30. Bevan, M. A.; Prieve, D. C. *Langmuir* **2000**, 16, 9274.

31. Fernandes, G. E.; Bevan, M. A. *Langmuir* **2007**, 23, 1500.

32. Kleshchanok, D.; Lang, P. R. *Langmuir* **2007**, 23, 4332.

33. Prieve, D. C. *Adv. Colloid Interface Sci.* **1999**, 82, 93.

34. Berne, B.; Pecora, R. Dynamic Light Scattering; Plenum: New York, **1976**.

35. Chu, B. Laser light Scattering 2nd ed; Academic: New York, **1991**.

36. Gao, J.; Wu, C. *Macromolecules* **1999**, 32, 1704.

37. Bahadur, P.; Pandya, K. *Langmuir* **1992**, 8, 2666.

38. Brown, W.; Schillen, K. *J. Phys. Chem.* **1992**, 96, 6038.

39. Jin, F.; Ye, J.; Hong, L. Z.; Lam, H. F.; Wu. C. *J. Phys. Chem. B* **2007**, 111, 2255.

40. Jin, F.; Li, J. F.; Ye, X. D.; Wu. C. *J. Phys. Chem. B* **2007**, 111, 11745.

41. Jin, F.; Ye, X. D.; Wu. C. *J. Phys. Chem. B* **2007**, 111, 13143.

42. Pagac, E. S.; Tilton, R. D.; Prieve, D. C. *Langmuir*, **1998**, 14, 5106.

43. Jin, F.; Gong, X. J.; Ngai, T. *Soft Matter*, **2008**, 4, 968.

44. Donnan, F. G.. Chem. Rev. **1924**, 1, 73.

45. Odiachi Jr, P. C.; Prieve, D. C. *Colloids and Surfaces A: Physicochem. Eng. Aspects* **1999**, 146, 315.

Chapter 4

pH-Controllable Depletion Attraction Induced by Microgel Particles

4.1 Introduction

As mentioned in Chapter 3, we have used the TIRM to investigate the nanobubble-induced depletion attraction between a sphere and flat surface in a solution consisting of polymeric, PEO-PPO-PEO surfactants [1,2]. The nanobubbles with size range around hundred nanometers were spontaneously formed. In addition, they could be reversibly removed by repeated filtration and regenerated by air injection so that we could directly measured the depletion force acting on the sphere by varying the aqueous solutions with or without the existence of nanobubbles, which could never be obtained in the conventional mixture of colloid and nonabsorbing polymers. However, since the size and concentration of nanobubbles were not under a well-controlled manner by spontaneously formation, the range and strength of depletion force could not be finely tuned.[24] Inspired by these limitations, in this study, we have synthesized the microgel particles, poly(*N*-isopropylacrylamide-*co*-methacrylic) (PNIPAM-*co*-MAA) which exhibits an extreme response to changes in solution pH and resulted in dramatic changes in microgel size. TIRM was then applied to directly measure the pH-triggered depletion interaction acting on a sphere immersed in the solution of such microgels close to a flat

glass surface.

4.2 Experimental Section

4.2.1 Sample Preparation

The PNIPAM-*co*-MAA microgels were synthesized by using surfactant-free precipitation polymerization, based on N-isopropylacrylamide as a monomer, cross-linked with N,N'-methylene bisarylamide, and of methacrylic acid (MAA) as a comonomer [3]. The incorporation of the carboxylic groups introduces a sensitivity to the pH, thus provides the trigger of the volume phase transition in PNIPAM-*co*-MAA microgels. Fig.4-1 shows that, for a given temperature, the hydrodynamic diameter of the PNIPAM-*co*-MAA microgels increases from 216 nm to 254 nm when pH of the solution is increased from 4.6 to 9.5. This is expected because the pH increase first induces the dissociation of carboxylic acid groups (-COOH) on the network chains, leading to increasing the charge density on the network. The concomitant increase in mobile counterion content of the network increases the internal osmotic pressure, which induces the swelling of microgel particles with a relatively broad size distribution [3,4]. Note that PNIPAM-based microgels are also well known to undergo the volume phase transition in water from a swollen state to a shrunken state by increasing the temperature [3]. However, for our synthesized microgels, we observed a very broad temperature change accompanied by small shrinkage in volume at both pH 4.6 and 9.5. The reason

of the broad temperature and small volume transition may be related to the inhomogeneous distribution of the comonomer in the PNIPAM-*co*-MAA copolymer microgels particularly with low MAA content [3]. Moreover, with the microgels being collapsed, the particle size is reduced, but the surface charge density is increased. When the charge density is high enough, for example at the high pH value, the microgels will not collapse further in increasing temperature, which explain why our synthesized microgels show a lower extent of shrinkage. Thus, in this study, we will investigate the effects of pH-triggered behavior of the PNIPAM-*co*-MAA microgels on the interaction potentials between the sphere and the flat surface by means of TIRM.

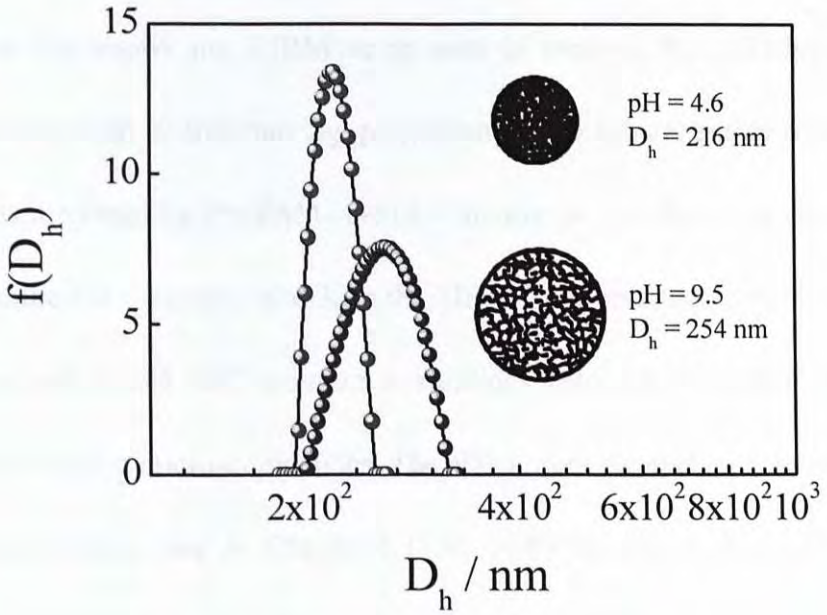

Fig.4-1 pH dependence of the hydrodynamic diameter (D_h) of PNIPAM -*co*-MAA microgels in an aqueous dispersion with microgel concentration of 10^{-5} g/ml at room temperature.

4.2.2 Total Internal Reflection Microscopy

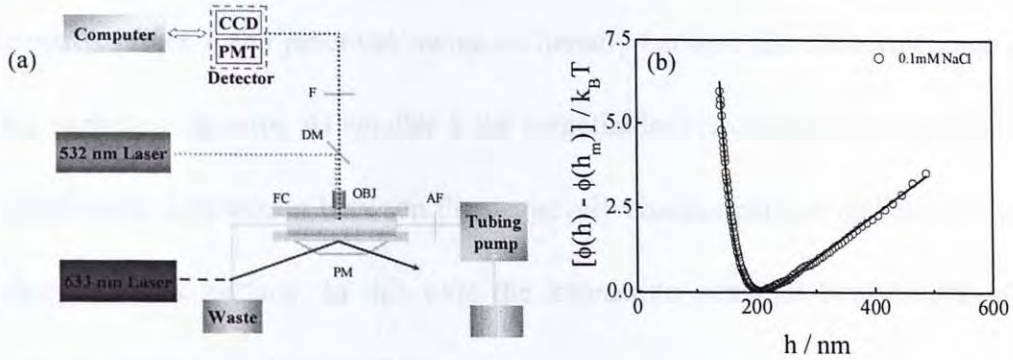

Fig.4-2 **a) The experimental setup used to directly measure the interaction between the polystyrene sphere and flat surface before and after the introduction of PNIPAM-*co*-MAA microgels, where FC = flow cell; PM = prism; OBJ = objective. b) The typical interaction potential between a charged PS sphere and a charged surface in 0.1 mM NaCl aqueous solution. The solid line is a theoretical fitted curve from Eq. 4.1.**

Fig.4-2(a) shows our T IRM setup used to measure the pH-triggered depletion potentials between a free-moving polystyrene (PS) sphere and a hydrophilic glass surface, as mediated by PNIPAM-*co*-MAA microgels. The details of this technique has been described in Chapter 2 and 3. In the TIRM force measurements, a very diluted PS dispersion in 0.1 mM NaCl solution was initially filled into a sample cell sandwiched between two silica microscopy slides. The slides were cleaned by following the normal procedures as described in Chapter 3 [5,6]. A PS sphere of average brightness was selected and held in place with optical tweezers by a solid-state Nd:YAG laser (output = 300mW at wavelength = 532 nm), while the rest of the spheres were flushed from the cell with NaCl aqueous solution. Once the excess spheres were washed away, the interaction potential between the single free-moving sphere and bare glass surface in 0.1

mM NaCl solution was recorded. Fig.2b shows that the interaction potential of the negatively charged PS sphere at height h above the glass plate is composed of two parts: towards larger h the potential increases linearly because the dominant force acting on the particle is gravity. At smaller h the potential increases exponentially because of the electrostatic interaction between the negatively charged particle and also the negatively charged silica surface. In this case the interaction potential between the sphere and surface can be described as [7,8]

$$\frac{\phi(h)}{k_B T} = Be^{-\kappa h} + \frac{G}{k_B T}h \tag{4.1}$$

where the amplitude of the electrostatic interaction B depends on the surface charges of the particle and the silica surface, κ^{-1} is Debye screening length of the solvent, and G is the weight of the particle. The solid line in the figure shows that the measured potential is well described by eq. 1, which also experimentally confirmed by several groups using TIRM [1,7,8].

After measure the interaction potential in pure NaCl solution, ~20 mL of deionized water was first used to rinse the sample cell, PNIPAM-*co*-MAA microgel dispersion then with different amount at pH 9.43 (adjusted by NaOH) were subsequently pumped into the cell by a flex tubing pump (Master Flex), while the PS sphere was trapped in place by tweezers. The trapped sphere was then released and the interaction potentials between the sphere and surface were measured with the presence of different amount of microgels in the swollen state. It is worthy to point out that the consecutive potentials are measured with the same PS sphere and same surface before and after

introduction the microgels, we thus can isolate the effect of existence microgels in the solution by comparison among the measured potentials.

4.3 Results and Discussion

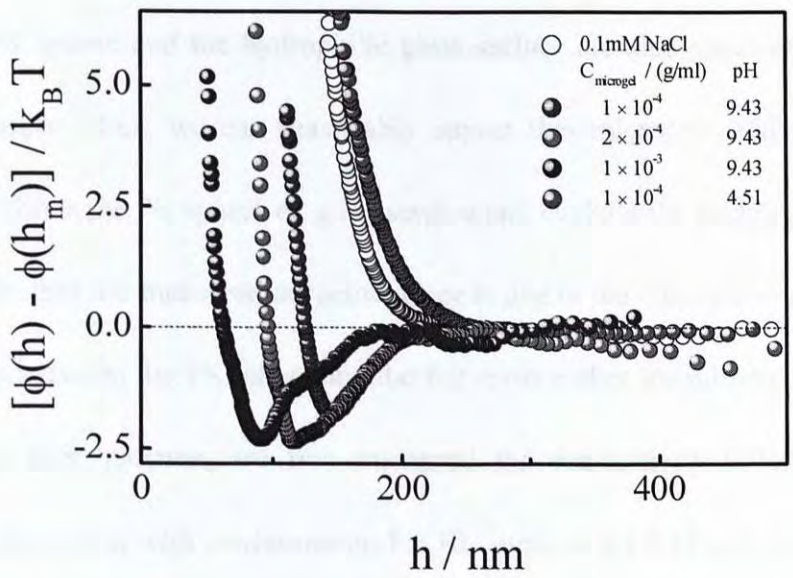

Fig.4-3 The measured interaction potentials (ϕ (h)/k_BT) between the polystyrene sphere and flat surface under different environmental conditions: namely, in 0.1mM NaCl aqueous solution, in different concentration microgel dispersion with pH = 9.43. Note that the gravity of all the interaction potentials has been subtracted.

Fig.4-3 shows that the interaction potentials between the PS sphere and surface with the presence of swollen microgels are significantly modified. Note that the contribution of the gravity has been subtracted from all potentials since the same PS sphere was used.

It clearly shows that addition of swollen microgels induce a long-range attractive force occurring at separation distances ranging from 150–250 nm, which may be contributed either to bridging or depletion. This attractive force is seen to increase with increasing swollen microgel concentration, while the separation distance decreases. Moreover, at higher swollen microgel volume fractions, the attractive well becomes narrow and steep, as well as acting over smaller separation distances. Note that the microgels with the pH 9.43 are negatively charged due to the dissociation of -COOH on the network chains. The selected PS sphere and the hydrophilic glass surface are also negatively charged in the measurements. Thus, we can reasonably expect that microgels will not preferentially absorb to either the PS sphere or glass surface and exclude the bridging effect. One may wonder whether the measured attractive force is due to the alternation of the electrostatic interaction between the PS sphere and the flat surface after the introduction of microgels. To answer this question, we first measured the conductivity (19 ± 0.2 μScm^{-1}) of microgel dispersion with concentration 1×10^{-4} g/mL at pH 9.43 and found that it is same as in a 0.1 mM NaCl aqueous solution. That means ionic strength or Debye length of the aqueous solution is similar before and after the introduction of microgels. The only different between the two solutions is the existence of microgels or not. To have an even clearer picture, we further calculated the surface potential between the PS sphere and the surface in the aqueous solution by applying the Eq. 4.1 to fit the measured potential profiles before and after introduction of swollen microgels. The fitting can result two parameters, namely, κ^{-1} and G. Note that Eq. 4.1, $\phi(h)$ has a minimum at a separation distance h_m given by [8]

$$\kappa h_m = \ln \frac{\kappa B}{G} \tag{4.2}$$

where h_m can be directly read from the measured potentials as shown in Fig.4-3 In this way, we can find the constant B which reflects the electrostatic repulsion potential between the two surfaces [8]. The values of lnB in 0.1 mM NaCl solution and microgel dispersion with pH 9.43 were determined as 9.0 and 13.1, respectively, indicating that the surface repulsion increases with the presence of swollen microgels. In other words, the separation distance between the PS sphere and surface is expected to be larger. However, it can be seen from Fig.4-3, our measured interaction potentials shift to a smaller distance with the existence of microgels. We therefore suggest that the measured attractive force likely caused by the exclusion or depletion the large swollen microgels from the gap between the PS sphere and the surface. At 0.1 mM NaCl solution, the separation distance between the sphere-surface (~220 nm) is smaller than the hydrodynamic diameter of the swollen microgels (~254 nm) under the condition of pH 9.43. The exclusion results in an osmotic pressure imbalance inside and outside the gap region, leading to the net attraction.

As mentioned above, the hydrodynamic volume of microgels can response to pH changes, one might expect the measured depletion attractive force to be a function of pH, too. To confirm such hypothesized pH dependence, we rinsed the sample cell with large amount of deionized water (changing the volume inside the cell at least 20 times) and then pumped the microgels with solution pH 4.51. Fig.4-3 shows that the measured long-range attractive force disappears, leaving only the electrostatic repulsion. We related

this effect to the collapsed microgels, with the hydrodynamic diameter smaller than the sphere-surface distance, are able to move into the gap region. The imbalance osmotic pressure inside and outside the region will disappear so as the depletion attractive force. Note that this attractive force can be regenerated by reintroduction of microgels at high pH condition and the process is reversible, which in turn indicates that microgel-triggered depletion attractive force is pH dependent as schematically summarized in Fig.4-4.

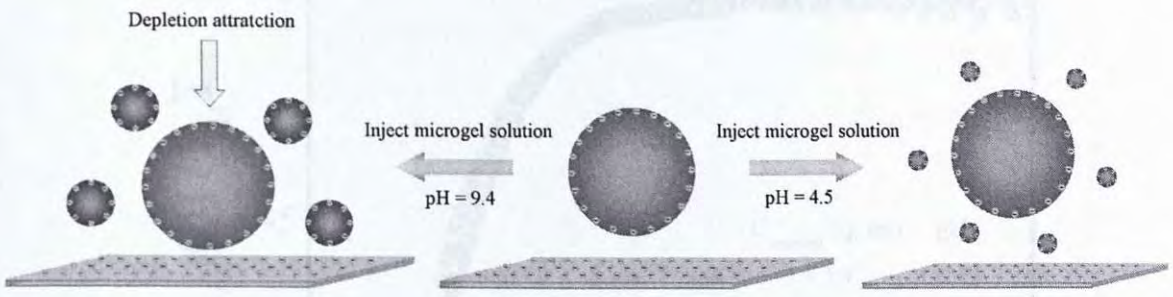

Fig.4-4 Schematic shows the pH-triggered depletion attraction acting on polystyrene sphere immersed in a microgel dispersion close to a flat surface.

To isolate the microgel-induced depletion potential and compare to theoretical mode, each measured potential at pH 9.43 was subtracted by potential at pH 4.51. The net depletion interactions were obtained and plotted in Fig.4-5. It clearly shows that the depletion attraction is continuous and with the measurable distance up to ~250 nm. The classical depletion potential function was used to fit the measured profiles shown in Fig.4-5, namely

$$\begin{aligned} \phi_{dep}(h) &= -\pi\Pi[(a+\Delta)(h-2\Delta)^2+\frac{1}{3}(h-2\Delta)^3] \quad for \quad 0<h<2\Delta \\ &= 0 \qquad\qquad\qquad\qquad\qquad\qquad\qquad\qquad for \quad h>2\Delta \end{aligned} \tag{4.3}$$

where Π is the osmotic pressure of the bulk solution, a is the radius of the polystyrene

particle (here a = 3.0 μm) and 2Δ is the depetion region [9]. The fitting gives 2Δ~250 nm and Π~0.4 pa. Note that the fitted depletion region can be compared to the hydrodynamic diameter of the swollen microgels, suggesting that our experimental results are in good agreement with the theoretical values predicated by Eq.4.3.

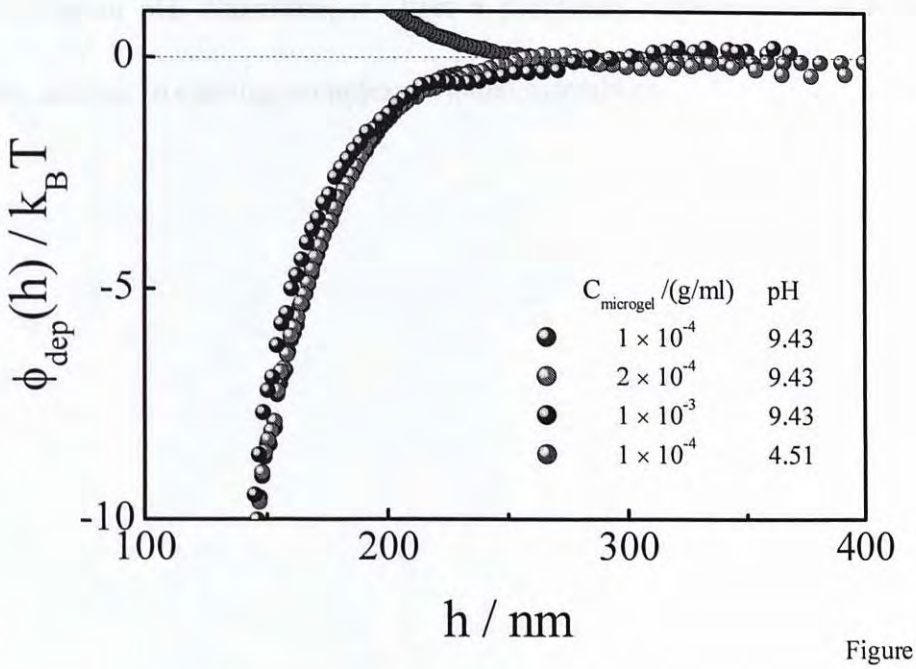

Figure 5

Fig.4-5 The measured depletion potentials between the polystyrene sphere and the flat surface with the presence of different amounts of swollen microgels.

4.4 Conclusion

In summary, we report first direct measurement of the pH-triggered depletion interaction potentials between a polystyrene sphere and a flat substrate as mediated by PNIPAM-*co*-MAA microgels. At high solution pH, an attractive force occurring at

separation distance of 150-250 nm was observed, which was seen to increase in magnitude with increasing microgel concentrations. The origin of this attractive force comes from exclusion or depletion the large swollen microgels between the gap of particle and flat surface. However, this depletion force disappeared as soon as changing the microgel dispersion to a low pH solution. The current study demonstrates the ability to quantitatively measure and reversibly control k_BT-scale depletion attraction as function of solution pH. Therefore, it offers a promising route to use such tunable depletion interactions in creating complex colloidal assemblies.

4.5 References and Notes

1. Jin, F.; Gong, X. J.; Ye, J.; Ngai, T. *Soft Matter*, **2008**, 4, 968.
2. Ngai, T.; Xing, X. C.; Jin, F., *Langmuir*, 2008, 24, 13912.
3. Zhou, S. Q.; Chu, B. *J. Phys. Chem. B* **1998**, 102, 1364.
4. Ngai, T.; Auweter, H.; Behrens, S. H. *Macromolecules*, **2006**, 39, 8171.
5. Jin, F.; Ye, J.; Hong, L. Z.; Lam, H. F.; Wu. C. *J. Phys. Chem. B* **2007**, 111, 2255.
6. Jin. F.; Li, J. F.; Ye, X. D.; Wu, C. *J. Phys. Chem. B* **2007**, 111, 11745.
7. Kleshchanok, D.; Lang, P. R. *Langmuir*, **2007**, 23, 4332.
8. Prieve, D. C. *Adv. Colloid Interface Sci.* **1999**, 82, 93.
9. Scheutjens, J. M. H. M.; Fleer, G. J. *J. Phys. Chem.* **1979**, *83*, 1619; **1980**, 84, 178.

Publication List

Ngai, T; Xing, X. C.; Fan, J. *Langmuir* **2008**, *24*, 13912.

Xing, X. C.; Li, Z. F.; Ngai, T. *Macromolecules submitted.*